

See discussions, stats, and author profiles for this publication at: <https://www.researchgate.net/publication/363878314>

Applications of a Group Theoretical Method on Biomagnetic Fluid Flow and Heat Transfer for Different Shapes of Fe₃O₄ Magnetic Particles under the Influence of Thermal Radiation and...

Article in Mathematics · September 2022

DOI: 10.3390/math10193520

CITATIONS

4

5 authors, including:



Md. Jahangir Alam
Comilla University
29 PUBLICATIONS 156 CITATIONS

[SEE PROFILE](#)

READS

170



Md. Ghulam Murtaza Talukder
Comilla University
69 PUBLICATIONS 365 CITATIONS

[SEE PROFILE](#)



Eugenia N. Petropoulou
University of Patras
41 PUBLICATIONS 191 CITATIONS

[SEE PROFILE](#)



Efstratios Tzirtzilakis
University of Peloponnese
96 PUBLICATIONS 1,922 CITATIONS

[SEE PROFILE](#)

Article

Applications of a Group Theoretical Method on Biomagnetic Fluid Flow and Heat Transfer for Different Shapes of Fe_3O_4 Magnetic Particles under the Influence of Thermal Radiation and a Magnetic Dipole over a Cylinder

Jahangir Alam ¹, Ghulam Murtaza ², Eugenia N. Petropoulou ³, Efstratios Em. Tzirtzilakis ^{4,*}  and Mohammad Ferdows ¹

¹ Research Group of Fluid Flow Modeling and Simulation, Department of Applied Mathematics, University of Dhaka, Dhaka 1000, Bangladesh

² Department of Mathematics, Comilla University, Cumilla 3506, Bangladesh

³ Geotechnical Engineering Laboratory, Department of Civil Engineering, University of Patras, 26500 Patras, Greece

⁴ Fluid Mechanics and Turbomachinery Laboratory, Department of Mechanical Engineering, University of the Peloponnese, 26334 Patras, Greece

* Correspondence: etzirtzilakis@uop.gr



Citation: Alam, J.; Murtaza, G.; Petropoulou, E.N.; Tzirtzilakis, E.E.; Ferdows, M. Applications of a Group Theoretical Method on Biomagnetic Fluid Flow and Heat Transfer for Different Shapes of Fe_3O_4 Magnetic Particles under the Influence of Thermal Radiation and a Magnetic Dipole over a Cylinder. *Mathematics* **2022**, *10*, 3520. <https://doi.org/10.3390/math10193520>

Academic Editors: Irina Cristea, Yuriy Rogovchenko, Justo Puerto, Gintautas Dzemyda and Patrick Siarry

Received: 29 August 2022

Accepted: 21 September 2022

Published: 27 September 2022

Publisher's Note: MDPI stays neutral with regard to jurisdictional claims in published maps and institutional affiliations.



Copyright: © 2022 by the authors. Licensee MDPI, Basel, Switzerland. This article is an open access article distributed under the terms and conditions of the Creative Commons Attribution (CC BY) license (<https://creativecommons.org/licenses/by/4.0/>).

Abstract: The flow and heat characteristics of an unsteady, laminar biomagnetic fluid, namely blood containing Fe_3O_4 magnetic particles, under the influence of thermal radiation and a magnetic dipole over a cylinder with controlled boundary conditions using a group theory method are investigated in the present study. The mathematical formulation of the problem is constructed with the aid of biomagnetic fluid dynamics (BFD) which combines principles of ferrohydrodynamics (FHD) and magnetohydrodynamics (MHD). It is assumed that blood exhibits polarization as well as electrical conductivity. Additionally, the shape of the magnetic particles, namely cylindrical and spherical, is also considered. Moreover, in this model, a group theoretical transformation, namely a two-parameter group technique, is applied. By applying this group transformation, the governing system of partial differential equations (PDEs) along with applicable boundary conditions are reduced to one independent variable and, consequently, converted into a system of ordinary differential equations (ODEs) with suitable boundary conditions. An efficient numerical technique is applied to solve the resultant ODEs and this technique is based on three essential features, namely (i) a common finite differences method with central differencing, (ii) tridiagonal matrix manipulation and (iii) an iterative procedure. The flow and heat characteristics of blood- Fe_3O_4 are found to be dependent on some physical parameters such as the particle volume fraction, the ferromagnetic interaction parameter, the magnetic field parameter, and the thermal radiation parameter. An ample parametric study is accomplished to narrate the influences of such physical parameters on velocity, temperature distributions as well as the coefficient of skin friction and rate of heat transfer. From the numerical results, it is deduced that the fluid velocity is enhanced for the ferromagnetic number and the temperature profile is decreased as the ferromagnetic number is gradually increased. It is also obtained that for the cylindrical shape of magnetic particles, the fluid temperature is more enhanced than that of the spherical shape. Both the skin friction coefficient and the local Nusselt number are increased for increasing values of the ferromagnetic interaction parameter, where the heat transfer rate of blood- Fe_3O_4 is significantly increased by approximately 33.2% compared to that of pure blood, whereas the coefficient of skin friction is reduced by approximately 6.82%.

Keywords: group theoretical method; biomagnetic fluid dynamics (BFD); blood; magnetic particles; cylinder; magnetic dipole; finite differences method

MSC: 35Q35; 76M20; 76M55; 76W05

1. Introduction

From a theoretical and practical point of view, the studies of biomagnetic fluid dynamics (BFD), which consists of the ideas of ferrohydrodynamics (FHD) and magnetohydrodynamics (MHD), exhibit much interest to researchers due to their variety of applications in biomedical and bio-engineering areas as reported early in [1–4] such as drug and gene delivery performed by magnetic particles, magnetic resonance imaging (MRI) for imaging, the reduction in blood during surgeries, cancer treatment, and injury treatment. For researchers in fluid dynamics, BFD is a comparatively new area, where the effect of the magnetic field on the biological fluid is studied. In the recent past, this area has received tremendous attention from researchers since it is directly related to non-invasive applications for treating human body-related diseases and disorders. Moreover, blood is considered as one of the peculiarities of BFD due to the presence of ions. Blood could be considered to behave as a Newtonian or non-Newtonian fluid. When blood flows at high shear rates through arteries, blood can be considered as a Newtonian fluid as mentioned by Chien et al. [5] and the true non-Newtonian nature of blood should be considered when shear rates are very low according to the study of Bhatti et al. [6].

The influence of a magnetic field is incorporated in the study of bio-fluids and that is why the concepts of FHD and MHD need to be introduced. Basically, in ferrohydrodynamics (FHD), fluid is considered electrically non-conducting, where fluid flows are influenced in the presence of magnetization by the polarization effect. Specifically, when a magnetic field is exposed to a magnetic fluid such as blood, a measurement of the magnetization can be made in order to determine how much is affected by the applied magnetic field. Magnetization can be described mathematically by involving the magnetic field strength intensity and/or temperature. On the other hand, in magnetohydrodynamics (MHD), the influence of magnetization is negligible and fluid flows like an electrically conducting magnetic fluid. Based on the above-mentioned concept, a mathematical study of BFD considering the FHD principles was initiated by Haik et al. [7], where fluid is considered as a Newtonian fluid. The authors found that in the presence of high-gradient magnetic fields, the flow of a biomagnetic fluid is significantly affected. This mathematical model was extended by Tzirtzikakis [8], where both principles, namely MHD and FHD, are considered simultaneously. The behavior of MHD blood flow under the effect of temperature-dependent fluid viscosity and thermal conductivity was investigated by Sharma et al. [9]. The impact of temperature-dependent magnetization on a non-Newtonian biomagnetic fluid using viscoelastic fluid property over a stretching sheet was studied by Misra et al. [10] and the numerical solution was obtained by using a finite differences technique. The influence of thermal radiation and slip conditions on time-dependent blood flow and heat transfer over an inclined permeable stretching surface was studied by Koppu et al. [11]. The dual behavior of blood flow and heat transfer in the quadratic stretched surface under the influence of a magnetic dipole was investigated by Murtaza et al. [12] and the authors reveal that, in a particular range of the suction parameter and stretching/shrinking sheet, the physical solutions, i.e., stable and unstable solutions, are present. Recently, the study of a biomagnetic fluid under the influence of a magnetic dipole was studied by Murtaza et al. [13], where it was shown that the combination of MHD and FHD, i.e., BFD flow, is comparatively more significant than that of MHD, FHD, or pure hydrodynamics flow alone.

In the recent past, many researchers investigated the study of different regular fluids (water, blood, etc.) by adding different types of nanoparticles (magnetic/non-magnetic). This is because the heat transfer of a base fluid like blood is significantly improved when nanoparticles are mixed with a base fluid and this improvement is more effective than conventional heat transfer in fluids where the size of nanoparticles is usually 1–100 nm. When nanoparticles are mixed with a base fluid, this is known as a nanofluid, initially introduced by Choi [14]. As far as cylinder flows have been concerned, Alsenafi and Ferdows [15] showed that depending on the systems' parameters, dual solutions exist in opposing flow beyond a critical point where both solutions are connected. The forced convection of a Al_2O_3 -water nanofluid over a circular cylinder inside a magnetic field was studied by

Nikelham et al. [16]. In that study, an experimental model as a function of the temperature, nanoparticle diameter, and volume fraction of the nanofluid was utilized to calculate the nanofluid's viscosity and conductivity coefficient. It was found that the model of the nanofluids is important, and the values of the Nusselt numbers in the experimental model are different than the Brinkman–Maxwell analytical one. Aminian et al. [17] numerically studied the MHD forced convection effects of Al_2O_3 –CuO–water nanofluid inside a partitioned cylinder within a porous medium. Nanofluid flow was modeled as a two-phase flow using a two-phase mixture model, and the Darcy–Brinkman–Forchheimer equation was employed to model fluid flow in porous media. They demonstrated that incorporation of nanoparticles to the base fluid increased the performance evaluation criteria in all cases. The MHD flow of water-based nanofluids across a horizontal circular cylinder was numerically investigated by Tlili et al. [18]. It was found that skin friction and the local Nusselt numbers are strong functions of Reynolds and Hartmann numbers, whereas the local Sherwood number is a strong function of nanofluids parameters. The impact of heat source/sink along with suction/injection on steady, two-dimensional MHD flow through a stretched cylinder was developed by Elbashbeshy et al. [19]. Finally, the unsteady magnetohydrodynamic mixed convection flow of an incompressible hybrid nanofluid (Cu – Al_2O_3 /water) past an isothermal cylinder with thermal radiation effect has been studied by Roy and Akter [20]. The corresponding results revealed that the hybrid nanofluid (Cu – Al_2O_3 /water) enhances the heat transfer by approximately 28.28% in comparison to the Al_2O_3 -water nanofluid and by approximately 51.15% more than in the pure fluid. Contrary to this, the heat transfer of hybrid nanofluid is augmented by approximately 41.76% more than the Cu-water nanofluid and by 71.41% more than the base fluid. The significance of melting in the presence of thermal radiation on Cattaneo–Christov-aligned MHD nanofluid flows together with microorganism to leading edge is investigated by Ali et al. [21] with an approaching FEM technique. An analysis of H_2O – Al_2O_3 nanofluid flow over a stretching sheet subject to prescribed heat flux in the presence of thermal radiation is studied by Kumar et al. [22]. They found that the coefficient of skin friction and thermal boundary layer decreases as the radius of nanoparticles is enhanced. Dawar et al. [23] examined the effects of Brownian motion and thermophoresis on MHD water-based nanofluid with copper and copper oxide nanoparticles between two parallel plates. It was found that the heat transfer rate is increased by approximately 1% between two blade-shaped nanoparticles as Cu and CuO when the values of volume fraction $\phi = 0.02$ and $\phi = 0.03$. Bilal et al. [24] inspected the $\text{C}_2\text{H}_6\text{O}_2$ – H_2O hybrid nanofluid flow with three different nanoparticles— TiO_2 , SiO_2 , and Al_2O_3 —with activation energy across two infinite parallel plates. They reported that when nanoparticles are added to a base fluid, the fluid velocity and the heat transfer rate increase. Souayeh et al. [25] performed a numerical analysis of the flow and heat transfer of water–silver/gold nanofluid flow through an electromagnetohydrodynamic (EMHD) peristaltic channel in the presence of activation energy and radiation and microorganisms. Alwawi et al. [26] applied the Keller box method solutions to recapitulate human blood and water with CuO, Al, Au nanoparticles assuming a constant surface heat flux subject to a circular cylinder. The authors reported that gold particles gave better numerical results compared to Aluminum and copper. The impact of a magnetic dipole on the flow and heat transfer of blood– $\text{MnZnFe}_2\text{O}_4$ over a cylinder is discussed by Alam et al. [27] with the help of a group theoretical method approach.

However, from the above-mentioned studies, the authors of the present paper observed that most of the research has been conducted with regular fluid by mixing non-magnetic particles. To the best of the authors' knowledge, although there are numerous studies on stretching sheet and stretching cylinder flows, there are not many studies on unsteady cylinder flow, where the base fluid (human blood) contains magnetic particles. The reason behind choosing magnetic particles rather than non-magnetic particles is the use of magnetic particles in medical applications, which is explained in [28–31]. The proposed mathematical model is that of BFD, which incorporates two principles, namely MHD and FHD, where blood is electrically conducting magnetic fluid which also exhibits magne-

tization. These two terms are interconnected. In most of the studies, researchers on the blood flow model only consider the magnetization effect, where the fluid is considered as an electrically non-conducting fluid. From a practical point of view, if we want to destroy the tumor cells from our body without harming good cells, we can apply a strong magnetic field in that particular tumor area and determine how much fluid is affected by this applied magnetic field, which is measured by the mathematical term known as magnetization. To solve such fluid mechanics problems, several transformation techniques have been proposed by various researchers. In this paper, a group theoretical method, namely a two-parameter group method, is applied to solve the blood-based magnetic particles problem over a cylinder under the influence of a magnetic dipole. By applying this two-parameter group theoretical method, we can find a group of solutions in terms of various conditions. Meanwhile, we are frequently in contact with previously derived analogous solutions and the two-parameter group restores many of these forms and we will find some completely new ones. Such group theoretical methodology, i.e., the one/two parameter group method, has been analyzed in [32–36]. By using this systematic method, the number of independent variables is reduced by one and, consequently, the governing partial differential equations (PDEs) are transformed into a set of ordinary differential equations (ODEs) along with suitable boundary conditions which are later numerically solved by applying an efficient numerical technique, based on a common finite differences method with tridiagonal matrix manipulation and an iterative procedure. The significant impact of involving parameters such as the ferromagnetic parameter, the magnetic particle volume fraction, the magnetic field parameter, thermal radiation, temperature profiles as well as the skin friction coefficient and the rate of heat transfer is discussed with their respective graphical outcomes. Two cases are considered for the obtained numerical solutions: the first case concerns the behavior of pure blood and blood- Fe_3O_4 , whereas the second solution examines the effect of particle shape on blood- Fe_3O_4 flow and heat transfer, which is also the key objective of the present study.

Furthermore, in this study, the maximum temperature for the human body is considered to be 41°C , which is reasonable for applications in cancer treatment and moreover noticeable for enzyme function and the function of other proteins of the human body. Therefore, the current study could be applicable to biomedical sciences especially in drug administration, cancer therapy, reducing the flow of blood during surgeries, etc. Since, this study relates to human body related diseases and disorders, it is hoped that it will be important not only for understanding flow mechanisms but also for taking prevention measures.

2. Mathematical and Physical Formulation

The schematic representation of the governing co-ordinate system considered in this study is presented in Figure 1. The fluid considered (blood) contains magnetic particles (Fe_3O_4) and flows through a two-dimensional cylinder along the \bar{x} -axis, where L is the characteristic length of the cylinder. The flow is considered as unsteady, and the cylinder has a radius \bar{R} and the \bar{r} -axis is the normal direction of the cylinder. The temperature of the cylinder surface is T_w and the ambient fluid temperature is T_c situated far away from the surface, with $T_w < T_c$. A magnetic dipole which is assumed to be located below the sheet maintaining a distance c , propagates a magnetic field of strength \bar{H} . Moreover, due to the presence of FHD principles, the base fluid (blood) exhibits the polarization effect, where the applied magnetic field is supposed to be strong enough, to attain the equilibrium of magnetization.

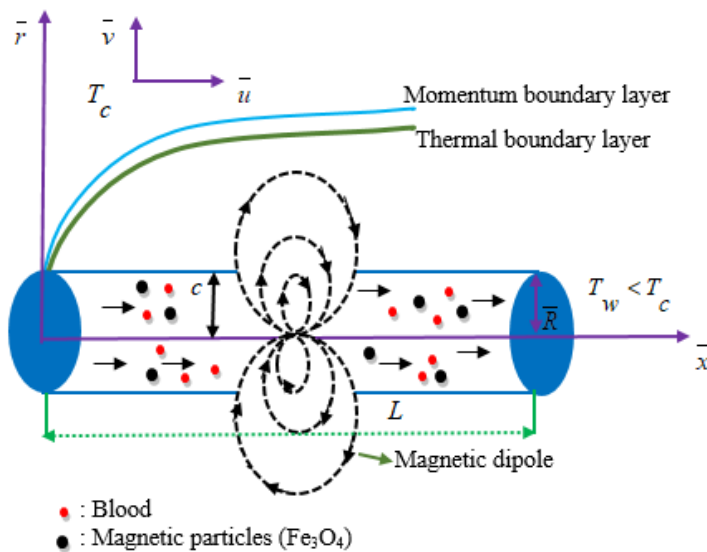


Figure 1. Schematic representation of geometry.

Due to the aforementioned assumptions and following [8,37], the governing continuity, momentum, and energy equations in cylindrical coordinates can be written as follows:

Continuity equation:

$$\frac{\partial \bar{u}}{\partial \bar{x}} + \frac{\bar{v}}{\bar{r}} + \frac{\partial \bar{v}}{\partial \bar{r}} = 0. \quad (1)$$

Momentum equation:

$$\frac{\partial \bar{u}}{\partial \bar{t}} + \bar{u} \frac{\partial \bar{u}}{\partial \bar{x}} + \bar{v} \frac{\partial \bar{u}}{\partial \bar{r}} = \frac{\mu_{mf}}{\rho_{mf}} \left(\frac{\partial^2 \bar{u}}{\partial \bar{r}^2} + \frac{1}{\bar{r}} \frac{\partial \bar{u}}{\partial \bar{r}} \right) - \frac{\sigma_{mf} B^2 \bar{u}}{\rho_{mf}} + \frac{\mu_0}{\rho_{mf}} M \frac{\partial \bar{H}}{\partial \bar{x}}. \quad (2)$$

Energy equation:

$$(\rho C_p)_{mf} \left(\frac{\partial \bar{T}}{\partial \bar{t}} + \bar{u} \frac{\partial \bar{T}}{\partial \bar{x}} + \bar{v} \frac{\partial \bar{T}}{\partial \bar{r}} \right) + \mu_0 \bar{T} \frac{\partial M}{\partial \bar{T}} \left(\bar{u} \frac{\partial \bar{H}}{\partial \bar{x}} + \bar{v} \frac{\partial \bar{H}}{\partial \bar{r}} \right) = \kappa_{mf} \left(\frac{\partial^2 \bar{T}}{\partial \bar{r}^2} + \frac{1}{\bar{r}} \frac{\partial \bar{T}}{\partial \bar{r}} \right) - \frac{\partial q_r}{\partial \bar{r}}. \quad (3)$$

The boundary conditions accompanying (1)–(3) are [27,35,37]:

$$\begin{aligned} \bar{r} = \bar{R} : \bar{u} = 0, \bar{v} = 0, \bar{T} = T_w, \\ \bar{r} \rightarrow \infty : \bar{u} = 0, \bar{T} = T_c. \end{aligned} \quad (4)$$

Here, \bar{u} and \bar{v} are the dimensional velocity components along the axis, respectively. Further, the symbols κ , ρ , C_p , μ , μ_0 , M , σ , \bar{H} , q_r are known as blood thermal conductivity, density, specific heat at constant pressure, dynamic viscosity, magnetic permeability, magnetization, electrical conductivity, magnetic field strength, and radiative heat flux, respectively. Additionally, $B (= \mu_0 \bar{H})$ is the magnetic induction and the subscript symbol $()_{mf}$ means magnetic fluid. The bar above the quantities indicates that the quantities are dimensional.

Due to the electrical conductivity of the fluid, the term $-\frac{\sigma_{mf} B^2 \bar{u}}{\rho_{mf}}$ arising in Equation (2), represents the Lorentz force per unit volume along the \bar{x} axis. This term is known from MHD studies [8,13]. From FHD studies [38–40], the component of the magnetic force per unit volume is defined by the term $\frac{\mu_0}{\rho_{mf}} M \frac{\partial \bar{H}}{\partial \bar{x}}$, arising in Equation (2) and depends on the existence of the magnetic gradients on the corresponding \bar{x} axis, while the thermal power per unit volume due to the magnetocaloric effect, is represented by the term $\mu_0 \bar{T} \frac{\partial M}{\partial \bar{T}} \left(\bar{u} \frac{\partial \bar{H}}{\partial \bar{x}} + \bar{v} \frac{\partial \bar{H}}{\partial \bar{r}} \right)$ arising in Equation (3).

Raptis [41,42] described the radiative heat flux q_r using Rosseland approximation in such a way that:

$$q_r = -\frac{4\sigma_1}{3\chi} \frac{\partial \bar{T}^4}{\partial \bar{r}}, \quad (5)$$

where σ_1 is the Stefan–Boltzmann constant and χ is the mean absorption coefficient. The fluid temperature differences within the flow are supposed to be sufficiently small. Then, the temperature term \bar{T}^4 may be expressed as a linear function of the temperature, by expanding \bar{T}^4 in a Taylor series about T_c and neglecting higher-order terms yielding the expression

$$\bar{T}^4 \cong 4T_c^3 \bar{T} - 3T_c^4. \quad (6)$$

Thus, the local radiant absorption is given by

$$\frac{\partial q_r}{\partial \bar{r}} = -\frac{16\sigma_1 T_c^3}{3\chi} \frac{\partial^2 \bar{T}}{\partial \bar{r}^2}. \quad (7)$$

Substituting (7) into Equation (3) yields

$$(\rho C_p)_{mf} \left(\frac{\partial \bar{T}}{\partial \bar{t}} + \bar{u} \frac{\partial \bar{T}}{\partial \bar{x}} + \bar{v} \frac{\partial \bar{T}}{\partial \bar{r}} \right) + \mu_0 \bar{T} \frac{\partial M}{\partial \bar{T}} \left(\bar{u} \frac{\partial \bar{H}}{\partial \bar{x}} + \bar{v} \frac{\partial \bar{H}}{\partial \bar{r}} \right) = \kappa_{mf} \left(\frac{\partial^2 \bar{T}}{\partial \bar{r}^2} + \frac{1}{\bar{r}} \frac{\partial \bar{T}}{\partial \bar{r}} \right) + \frac{16\sigma_1 T_c^3}{3\chi} \frac{\partial^2 \bar{T}}{\partial \bar{r}^2} \quad (8)$$

According to [43,44], the components \bar{H}_x and \bar{H}_r of the magnetic field $\vec{\bar{H}} = (\bar{H}_x, \bar{H}_r)$, due to the magnetic dipole may be written as follows:

$$\bar{H}_x(\bar{x}, \bar{r}) = -\frac{\partial V}{\partial \bar{x}} = \frac{\gamma}{2\pi} \frac{\bar{x}^2 - (\bar{r} + c)^2}{(\bar{x}^2 + (\bar{r} + c)^2)^2}, \quad (9)$$

$$\bar{H}_r(\bar{x}, \bar{r}) = -\frac{\partial V}{\partial \bar{r}} = \frac{\gamma}{2\pi} \frac{2\bar{x}(\bar{r} + c)}{(\bar{x}^2 + (\bar{r} + c)^2)^2}, \quad (10)$$

where the scalar potential of the magnetic dipole is defined by $V(\bar{x}, \bar{r}) = \frac{\gamma}{2\pi} \frac{\bar{x}}{\bar{x}^2 + (\bar{r} + c)^2}$ and γ is the strength of the magnetic field at the source position. The magnetic field strength intensity \bar{H} is given by

$$\bar{H}(\bar{x}, \bar{r}) = \sqrt{\bar{H}_x^2 + \bar{H}_r^2} = \frac{\gamma}{2\pi} \frac{1}{\bar{x}^2 + (\bar{r} + c)^2}, \quad (11)$$

and the gradients of the magnetic field intensity are obtained by the above relation by expanding \bar{H} in powers of \bar{x} and retaining terms up to \bar{x}^2 , taking eventually the form

$$\frac{\partial \bar{H}}{\partial \bar{x}} = -\frac{\gamma}{2\pi} \frac{2\bar{x}}{(\bar{r} + c)^4}, \quad (12)$$

$$\frac{\partial \bar{H}}{\partial \bar{r}} = -\frac{\gamma}{2\pi} \left(\frac{-2}{(\bar{r} + c)^3} + \frac{4\bar{x}^2}{(\bar{r} + c)^5} \right). \quad (13)$$

Moreover, Matsuki et al. [45] experimentally showed that the magnetization M can be expressed as a function of the temperature \bar{T} and the magnetic field strength intensity \bar{H} is given by

$$M = K \bar{H} (T_c - \bar{T}), \quad (14)$$

where K is the pyromagnetic coefficient and T_c is the Curie temperature.

The thermophysical properties of the base fluid and magnetic particles are introduced according to the studies of Makinde [46], Lin et al. [47] and Kandasamy et al. [48] and presented in Table 1.

Table 1. Thermophysical properties of the magnetic fluid model [46–48].

Magnetic Fluid Properties	Applied Model
Density	$\rho_{mf} = (1 - \phi)\rho_f + \phi\rho_s$
Dynamic viscosity	$\mu_{mf} = \mu_f (1 - \phi)^{-2.5}$
Electrical conductivity	$\frac{\sigma_{mf}}{\sigma_f} = 1 + \frac{3 \left(\frac{\sigma_s}{\sigma_f} - 1 \right) \phi}{\left(\frac{\sigma_s}{\sigma_f} + 1 \right) - \left(\frac{\sigma_s}{\sigma_f} - 1 \right) \phi}$
Heat capacitance	$(\rho C_p)_{mf} = (1 - \phi)(\rho C_p)_f + \phi(\rho C_p)_s$
Thermal conductivity	$\frac{\kappa_{mf}}{\kappa_f} = \frac{(\kappa_s + (m-1)\kappa_f) - (m-1)\phi(\kappa_f - \kappa_s)}{(\kappa_s + (m-1)\kappa_f) + \phi(\kappa_f - \kappa_s)}$

Here, ϕ denotes the magnetic particle volume fraction and m is the magnetic particle shape factor such that when $m = 3$ and $m = 6.3698$ represent that the particles have spherical and cylindrical shape, respectively. Further, the notations $()_f$ and $()_s$ stand for the base fluid and the magnetic particles, respectively. When $\phi = 0$, all corresponding equations are transformed into a regular fluid model. In this paper, blood is considered as the base fluid and Fe_3O_4 as the magnetic particles and their corresponding thermophysical properties are tabulated in Table 2 according to previous studies [49–51].

Table 2. The values of thermophysical properties of blood and Fe_3O_4 [49–51].

Physical properties	$C_p \left(\text{jkg}^{-1}\text{K}^{-1} \right)$	$\rho \left(\text{kgm}^{-3} \right)$	$\sigma \left(\text{sm}^{-1} \right)$	$\kappa \left(\text{Wm}^{-1}\text{K}^{-1} \right)$
Blood	3.9×10^3	1050	0.8	0.5
Fe_3O_4	670	5180	0.74×10^6	9.7

In order to proceed with the solution of the problem, Equations (1), (2) and (8) together with the boundary conditions (4) are transformed into dimensionless form by using the following transformations [27,35,37]:

$$x = \frac{\bar{x}}{\bar{R}}, r = \frac{\bar{r}}{\bar{R}}, u = \frac{\bar{u}}{\bar{v}_f} \bar{R}, v = \frac{\bar{v}}{\bar{v}_f} \bar{R}, t = \frac{\bar{t}}{\bar{R}^2}, H = \frac{\bar{H}}{H_0}, \theta = \frac{T_c - \bar{T}}{T_c - T_w}, \quad (15)$$

where v_f is the kinematic viscosity of the fluid and H_0 is the reference magnetic field strength intensity. Hence, the reduced dimensionless form of the corresponding equations with boundary conditions are:

$$\frac{\partial u}{\partial x} + \frac{v}{r} + \frac{\partial v}{\partial r} = 0, \quad (16)$$

$$A_1 \left(\frac{\partial u}{\partial t} + u \frac{\partial u}{\partial x} + v \frac{\partial u}{\partial r} \right) = \frac{\partial^2 u}{\partial r^2} + \frac{1}{r} \frac{\partial u}{\partial r} - A_2 M n H^2 u + A_3 \beta H \theta \frac{\partial H}{\partial x}, \quad (17)$$

$$A_4 \text{Pr} \left(\frac{\partial \theta}{\partial t} + u \frac{\partial \theta}{\partial x} + v \frac{\partial \theta}{\partial r} \right) + A_5 \beta E c H (\varepsilon - \theta) \left(u \frac{\partial H}{\partial x} + v \frac{\partial H}{\partial r} \right) = (1 + N r A_5) \frac{\partial^2 \theta}{\partial r^2} + \frac{1}{r} \frac{\partial \theta}{\partial r}, \quad (18)$$

$$\begin{aligned} r = 1 : & u = 0, v = 0, \theta = 1 \\ r \rightarrow \infty : & u = 0, \theta = 0 \end{aligned} \quad (19)$$

where

$$A_1 = (1 - \phi)^{2.5} \left(1 - \phi + \phi \frac{\rho_s}{\rho_f}\right), A_2 = (1 - \phi)^{2.5} \left[1 + \frac{3 \left(\frac{\sigma_s}{\sigma_f} - 1\right) \phi}{\left(\frac{\sigma_s}{\sigma_f} + 1\right) - \left(\frac{\sigma_s}{\sigma_f} - 1\right) \phi}\right], \\ A_3 = (1 - \phi)^{2.5}, A_4 = \frac{\kappa_f}{\kappa_{mf}} \left(1 - \phi + \phi \frac{(\rho C_p)_s}{(\rho C_p)_f}\right), A_5 = \frac{\kappa_f}{\kappa_{mf}} \quad (20)$$

Here, $\beta = \frac{\mu_0 K H_0^2 (T_c - T_w) \bar{R}^2 \rho_f}{\mu_f^2}$ is the ferromagnetic interaction parameter, $Mn = \frac{\sigma_f \mu_0^2 H_0^2 \bar{R}^2}{\mu_f}$ is the magnetic field parameter, $Nr = \frac{16 \sigma_1 T_c^3}{3 \chi \kappa_f}$, is the thermal radiation parameter, $Pr = \frac{(\mu C_p)_f}{\kappa_f}$, is the Prandtl number, $\varepsilon = \frac{T_c}{T_c - T_w}$ is the dimensionless Curie temperature and $Ec = \frac{\mu_f^3}{\rho_f^2 \kappa_f \bar{R}^2 (T_c - T_w)}$ is the Eckert number.

If the stream function ψ formulation is adopted, i.e., define the velocity components as

$$u = \frac{1}{r} \frac{\partial \psi}{\partial r}, v = -\frac{1}{r} \frac{\partial \psi}{\partial x}$$

Equation (16) is automatically satisfied and Equations (17) and (18) take the form:

$$A_1 \left[r^2 \frac{\partial^2 \psi}{\partial t \partial r} + r \frac{\partial \psi}{\partial r} \frac{\partial^2 \psi}{\partial x \partial r} + \frac{\partial \psi}{\partial x} \left(\frac{\partial \psi}{\partial r} - r \frac{\partial^2 \psi}{\partial r^2} \right) \right] = r^2 \frac{\partial^3 \psi}{\partial r^3} - r \frac{\partial^2 \psi}{\partial r^2} + \frac{\partial \psi}{\partial r} \\ - A_2 Mn H^2 r^2 \frac{\partial \psi}{\partial r} + A_3 \beta H r^3 \theta \frac{\partial H}{\partial x} \quad (21)$$

$$A_4 Pr \left(r \frac{\partial \theta}{\partial t} + \frac{\partial \psi}{\partial r} \frac{\partial \theta}{\partial x} - \frac{\partial \psi}{\partial x} \frac{\partial \theta}{\partial r} \right) + A_5 \beta Ec H (\varepsilon - \theta) \left(\frac{\partial \psi}{\partial r} \frac{\partial H}{\partial x} - \frac{\partial \psi}{\partial x} \frac{\partial H}{\partial r} \right) = (1 + Nr A_5) r \frac{\partial^2 \theta}{\partial r^2} + \frac{\partial \theta}{\partial r}, \quad (22)$$

along with the boundary conditions:

$$r = 1 : \frac{\partial \psi}{\partial r} = 0, \frac{\partial \psi}{\partial x} = 0, \theta = 1 \\ r \rightarrow \infty : \frac{\partial \psi}{\partial r} = 0, \theta = 0 \quad (23)$$

3. The Group of Transformations

To identify all symmetries of a given differential equation (DE), group method analysis is the only rigorous mathematical method and for that no prior knowledge or exceptional assumptions of the given boundary layer equations under inquisition is needed. In physical standpoint, the boundary layer equations are very interesting due to their potency to admit a huge number of analytic solutions, i.e., invariant solutions. Here, invariant solutions mean the reduction of PDEs to simpler ODEs. Basically, the researchers in the fluid mechanics field, try to obtain similarity solutions by proposing a general similarity transformation with unknown parameters into the DE and as a result get an algebraic system. Then, the solution of this system, if it exists, determines the values of the unknown parameters. From this point of view, we believe that it is better to attack any problem of similarity solutions from the outset; that is, to find out the full list of symmetries of the problem and then study which of them are appropriate to provide group-invariant solutions more specifically similarity solutions. The two-parameter method that we applied in this model provided a group of solutions which is one of the major advantages of this group method. However, few limitations of this method also hold, such as the large number of arbitrary coefficients appearing in the obtained ODEs. It is quite difficult to determine numerical solutions to the problem.

In this section, a group theoretical method is applied to the system of PDEs (21)–(22) along with the boundary conditions (23). More precisely, a two-parameter transformation group is applied, which reduces the number of independent variables by one. Consequently, the set of PDEs (21)–(22) is converted into a system of ODEs.

3.1. The Group Systematic Formulation

The procedure is initiated with a class G of two-parameter (a_1, a_2) transformation group of the form

$$G : \bar{S} = C^S(a_1, a_2) S + K^S(a_1, a_2), \quad (24)$$

where C^S and K^S are real values and at least differentiable in each argument (a_1, a_2) and the symbol S stands for x, r, t, ψ, θ, H . Relation (24) may be further expressed in the following way:

$$G : \begin{cases} \bar{x} = C^x(a_1, a_2) x + K^x(a_1, a_2) \\ \bar{r} = C^r(a_1, a_2) r + K^r(a_1, a_2) \\ \bar{t} = C^t(a_1, a_2) t + K^t(a_1, a_2) \\ \bar{\psi} = C^\psi(a_1, a_2) \psi + K^\psi(a_1, a_2) \\ \bar{\theta} = C^\theta(a_1, a_2) \theta + K^\theta(a_1, a_2) \\ \bar{H} = C^H(a_1, a_2) H + K^H(a_1, a_2) \end{cases}, \quad (25)$$

which possesses complete sets of absolute invariants η (x, r, t) and ξ_i (x, r, t, ψ, θ, H), $i = 1, 2, 3$ where ξ_i are the three absolute invariants corresponding to ψ, θ, H . If η is the absolute invariant of the independent variables, then $\xi_i = F_i(\eta)$, $i = 1, 2, 3$. For more details one may refer to [52] or [53].

3.2. The Invariance Analysis

The transformation for the derivatives appearing in Equations (21) to (23), are directly gained from G via chain-rule operations and are

$$\frac{\partial \bar{S}}{\partial i} = \frac{C^S}{C^i} \frac{\partial S}{\partial i} \frac{\partial^2 \bar{S}}{\partial i^2} = \frac{C^S}{(C^i)^2} \frac{\partial^2 S}{\partial i^2} \frac{\partial^3 \bar{S}}{\partial i^3} = \frac{C^S}{(C^i)^3} \frac{\partial^3 S}{\partial i^3} \frac{\partial^2 \bar{S}}{\partial i \partial j} = \frac{C^S}{C^i C^j} \frac{\partial^2 S}{\partial i \partial j}, \quad (26)$$

where $S = \psi, \theta, H$ and $i, j = x, r, t$.

Equation (21) is said to be invariantly transformed under (25) and (26), whenever

$$\begin{aligned} A_1 & \left\{ \bar{r}^2 \frac{\partial^2 \bar{\psi}}{\partial \bar{t} \partial \bar{r}} + \bar{r} \frac{\partial \bar{\psi}}{\partial \bar{r}} \frac{\partial^2 \bar{\psi}}{\partial \bar{x} \partial \bar{r}} + \frac{\partial \bar{\psi}}{\partial \bar{x}} \left(\frac{\partial \bar{\psi}}{\partial \bar{r}} - \bar{r} \frac{\partial^2 \bar{\psi}}{\partial \bar{r}^2} \right) \right\} - \frac{\partial \bar{\psi}}{\partial \bar{r}} + \bar{r} \frac{\partial^2 \bar{\psi}}{\partial \bar{r}^2} - \bar{r}^2 \frac{\partial^3 \bar{\psi}}{\partial \bar{r}^3} + A_2 M n \bar{H}^2 \bar{r}^2 \frac{\partial \bar{\psi}}{\partial \bar{r}} \\ & - A_3 \beta \bar{H} \bar{r}^3 \bar{\theta} \frac{\partial \bar{H}}{\partial \bar{x}} = I_1(a_1, a_2) \left[\begin{aligned} & A_1 \left\{ r^2 \frac{\partial^2 \psi}{\partial t \partial r} + r \frac{\partial \psi}{\partial r} \frac{\partial^2 \psi}{\partial x \partial r} + \frac{\partial \psi}{\partial x} \left(\frac{\partial \psi}{\partial r} - r \frac{\partial^2 \psi}{\partial r^2} \right) \right\} \\ & - \frac{\partial \psi}{\partial r} + r \frac{\partial^2 \psi}{\partial r^2} - r^2 \frac{\partial^3 \psi}{\partial r^3} + A_2 M n H^2 r^2 \frac{\partial \psi}{\partial r} - A_3 \beta H r^3 \theta \frac{\partial H}{\partial x} \end{aligned} \right] \end{aligned} \quad (27)$$

for some function $I_1(a_1, a_2)$ which may be constant. The terms defined in (25) together with the corresponding derivatives from (26) are substituted into the left side of Equation (27), yielding

$$\begin{aligned} A_1 & \left[\frac{C^\psi C^r}{C^t} r^2 \frac{\partial^2 \psi}{\partial t \partial r} + \frac{(C^\psi)^2}{C^x C^r} r \frac{\partial \psi}{\partial r} \frac{\partial^2 \psi}{\partial x \partial r} + \frac{(C^\psi)^2}{C^x C^r} \frac{\partial \psi}{\partial x} \left(\frac{\partial \psi}{\partial r} - r \frac{\partial^2 \psi}{\partial r^2} \right) \right] - \frac{C^\psi}{C^r} \frac{\partial \psi}{\partial r} \\ & + \frac{C^\psi}{C^r} r \frac{\partial^2 \psi}{\partial r^2} - \frac{C^\psi}{C^r} r^2 \frac{\partial^3 \psi}{\partial r^3} + A_2 C^\psi C^r (C^H)^2 M n H^2 r^2 \frac{\partial \psi}{\partial r} - A_3 \frac{C^\theta (C^H)^2 (C^r)^3}{C^x} \\ & \beta H r^3 \theta \frac{\partial H}{\partial x} + R_1(a_1, a_2) = I_1(a_1, a_2) \left[A_1 \left\{ r^2 \frac{\partial^2 \psi}{\partial t \partial r} + r \frac{\partial \psi}{\partial r} \frac{\partial^2 \psi}{\partial x \partial r} + \frac{\partial \psi}{\partial x} \left(\frac{\partial \psi}{\partial r} - r \frac{\partial^2 \psi}{\partial r^2} \right) \right\} \right. \\ & \left. - \frac{\partial \psi}{\partial r} + r \frac{\partial^2 \psi}{\partial r^2} - r^2 \frac{\partial^3 \psi}{\partial r^3} + A_2 M n H^2 r^2 \frac{\partial \psi}{\partial r} - A_3 \beta H r^3 \theta \frac{\partial H}{\partial x} \right] \end{aligned} \quad (28)$$

where

$$\begin{aligned}
R_1(a_1, a_2) = & A_1 \left[\left\{ 2C^r K^r r + (K^r)^2 \right\} \frac{C^\psi}{C^t C^r} \frac{\partial^2 \psi}{\partial t \partial r} + \frac{(C^\psi)^2}{C^x (C^r)^2} K^r \frac{\partial \psi}{\partial r} \frac{\partial^2 \psi}{\partial x \partial r} - \frac{(C^\psi)^2}{C^x (C^r)^2} K^r \frac{\partial \psi}{\partial x} \frac{\partial^2 \psi}{\partial r^2} \right] + \frac{C^\psi}{(C^r)^2} \\
& K^r \frac{\partial^2 \psi}{\partial r^2} - \left\{ 2C^r K^r r + (K^r)^2 \right\} \frac{C^\psi}{(C^r)^3} \frac{\partial^3 \psi}{\partial r^3} + A_2 M n \left[\left\{ 2C^r K^r r + (K^r)^2 \right\} \frac{C^\psi (C^H)^2}{C^r} H^2 \frac{\partial \psi}{\partial r} + \right. \\
& \left. \left\{ 2C^H K^H H + (K^H)^2 \right\} \left\{ C^\psi C^r r^2 \frac{\partial \psi}{\partial r} + \left\{ 2C^r K^r r + (K^r)^2 \right\} \frac{C^\psi}{C^r} \frac{\partial \psi}{\partial r} \right\} \right] - \frac{(C^r)^3 C^\theta C^H}{C^x} K^H A_3 \beta r^3 \theta \frac{\partial H}{\partial x} \\
& - \frac{(C^r)^3 (C^H)^2}{C^x} K^\theta A_3 H \beta r^3 \frac{\partial H}{\partial x} - \frac{(C^r)^3 C^H K^\theta}{C^x} K^H A_3 \beta r^3 \frac{\partial H}{\partial x} - \left[3(C^r r)^2 K^r + 3C^r r (K^r)^2 + (K^r)^3 \right] \\
& \left[\frac{(C^H)^2 C^\theta}{C^x} A_3 \beta H \theta \frac{\partial H}{\partial x} + \frac{C^\theta C^H}{C^x} K^H A_3 \beta \theta \frac{\partial H}{\partial x} + \frac{(C^H)^2 K^\theta}{C^x} A_3 \beta H \frac{\partial H}{\partial x} + \frac{C^H K^\theta}{C^x} K^H A_3 \beta \frac{\partial H}{\partial x} \right]. \tag{29}
\end{aligned}$$

From the form of Equation (28), it is obvious that (28) is invariantly transformed whenever

$$I_1(a_1, a_2) = \frac{C^\psi C^r}{C^t} = \frac{(C^\psi)^2}{C^x C^r} = \frac{C^\psi}{C^r} = C^\psi C^r (C^H)^2 = \frac{C^\theta (C^H)^2 (C^r)^3}{C^x}, \tag{30}$$

and $R_1(a_1, a_2) \equiv 0$, which implies

$$K^r \equiv K^H \equiv K^\theta \equiv 0. \tag{31}$$

Similarly, Equation (22) is invariantly transformed under (25) and (26), by assuming that for some function $I_2(a_1, a_2)$, which may be constant the following holds:

$$\begin{aligned}
& A_4 \text{Pr} \left(\bar{r} \frac{\partial \bar{\theta}}{\partial \bar{t}} + \frac{\partial \bar{\psi}}{\partial \bar{r}} \frac{\partial \bar{\theta}}{\partial \bar{x}} - \frac{\partial \bar{\psi}}{\partial \bar{x}} \frac{\partial \bar{\theta}}{\partial \bar{r}} \right) + A_5 \beta E c \varepsilon \bar{H} \left(\frac{\partial \bar{\psi}}{\partial \bar{r}} \frac{\partial \bar{H}}{\partial \bar{x}} - \frac{\partial \bar{\psi}}{\partial \bar{x}} \frac{\partial \bar{H}}{\partial \bar{r}} \right) \\
& - A_5 \beta E c \bar{H} \theta \left(\frac{\partial \bar{\psi}}{\partial \bar{r}} \frac{\partial \bar{H}}{\partial \bar{x}} - \frac{\partial \bar{\psi}}{\partial \bar{x}} \frac{\partial \bar{H}}{\partial \bar{r}} \right) - \left\{ (1 + N r A_5) \bar{r} \frac{\partial^2 \bar{\theta}}{\partial \bar{r}^2} + \frac{\partial \bar{\theta}}{\partial \bar{r}} \right\} \\
& = I_2(a_1, a_2) \left[A_4 \text{Pr} \left(r \frac{\partial \theta}{\partial t} + \frac{\partial \psi}{\partial r} \frac{\partial \theta}{\partial x} - \frac{\partial \psi}{\partial x} \frac{\partial \theta}{\partial r} \right) + A_5 \beta E c \varepsilon H \left(\frac{\partial \psi}{\partial r} \frac{\partial H}{\partial x} - \frac{\partial \psi}{\partial x} \frac{\partial H}{\partial r} \right) \right] \\
& - A_5 \beta E c H \theta \left(\frac{\partial \psi}{\partial r} \frac{\partial H}{\partial x} - \frac{\partial \psi}{\partial x} \frac{\partial H}{\partial r} \right) - \left\{ (1 + N r A_5) r \frac{\partial^2 \theta}{\partial r^2} + \frac{\partial \theta}{\partial r} \right\} \tag{32}
\end{aligned}$$

Substitution of (24)–(26) into the left side of Equation (32) gives

$$\begin{aligned}
& A_4 \text{Pr} \left[\frac{C^r C^\theta}{C^t} r \frac{\partial \theta}{\partial t} + \frac{C^\psi C^\theta}{C^r C^x} \left(\frac{\partial \psi}{\partial r} \frac{\partial \theta}{\partial x} - \frac{\partial \psi}{\partial x} \frac{\partial \theta}{\partial r} \right) \right] + \frac{C^\psi (C^H)^2}{C^r C^x} A_5 \beta E c \varepsilon H \left(\frac{\partial \psi}{\partial r} \frac{\partial H}{\partial x} - \frac{\partial \psi}{\partial x} \frac{\partial H}{\partial r} \right) \\
& - \frac{C^\psi C^\theta (C^H)^2}{C^r C^x} A_5 \beta E c H \theta \left(\frac{\partial \psi}{\partial r} \frac{\partial H}{\partial x} - \frac{\partial \psi}{\partial x} \frac{\partial H}{\partial r} \right) - \frac{C^\theta}{C^r} \left\{ (1 + N r A_5) r \frac{\partial^2 \theta}{\partial r^2} + \frac{\partial \theta}{\partial r} \right\} + R_2(a_1, a_2) \\
& = I_2(a_1, a_2) \left[A_4 \text{Pr} \left(r \frac{\partial \theta}{\partial t} + \frac{\partial \psi}{\partial r} \frac{\partial \theta}{\partial x} - \frac{\partial \psi}{\partial x} \frac{\partial \theta}{\partial r} \right) + A_5 \beta E c \varepsilon H \left(\frac{\partial \psi}{\partial r} \frac{\partial H}{\partial x} - \frac{\partial \psi}{\partial x} \frac{\partial H}{\partial r} \right) \right], \\
& - A_5 \beta E c H \theta \left(\frac{\partial \psi}{\partial r} \frac{\partial H}{\partial x} - \frac{\partial \psi}{\partial x} \frac{\partial H}{\partial r} \right) - \left\{ (1 + N r A_5) r \frac{\partial^2 \theta}{\partial r^2} + \frac{\partial \theta}{\partial r} \right\}, \tag{33}
\end{aligned}$$

where

$$\begin{aligned}
R_2(a_1, a_2) = & A_4 \text{Pr} \frac{C^\theta K^r}{C^t} \frac{\partial \theta}{\partial t} + \frac{C^\psi C^H K^H}{C^r C^x} A_5 \beta E c \varepsilon \left(\frac{\partial \psi}{\partial r} \frac{\partial H}{\partial x} - \frac{\partial \psi}{\partial x} \frac{\partial H}{\partial r} \right) \\
& - A_5 \beta E c \left[\frac{C^\psi K^\theta (C^H)^2}{C^r C^x} H + \frac{C^\psi C^\theta C^H K^\theta}{C^x C^r} \theta + \frac{C^\psi C^H K^H K^\theta}{C^x C^r} \right] \\
& \left(\frac{\partial \psi}{\partial r} \frac{\partial H}{\partial x} - \frac{\partial \psi}{\partial x} \frac{\partial H}{\partial r} \right) - \frac{C^\theta}{(C^r)^2} K^r (1 + N r A_5) \frac{\partial^2 \theta}{\partial r^2}. \tag{34}
\end{aligned}$$

From (33), it is obvious that it is invariantly transformed whenever

$$I_2(a_1, a_2) = \frac{C^\theta C^r}{C^t} = \frac{C^\theta C^\psi}{C^x C^r} = \frac{C^\theta}{C^r} = \frac{C^\psi (C^H)^2}{C^x C^r} = \frac{C^\theta C^\psi (C^H)^2}{C^x C^r}, \quad (35)$$

and $R_2(a_1, a_2) \equiv 0$, which implies

$$K^r \equiv K^H \equiv K^\theta \equiv 0. \quad (36)$$

Finally, the boundary conditions (23) must also be invariant under the same transformations, which yields

$$C^r = 1 \text{ and } C^\theta = 1. \quad (37)$$

Combining Equations (30) and (35) and taking into account (31), (36), and (37), it was found that:

$$C^t = 1 \text{ and } C^x = C^H = C^\psi = 1. \quad (38)$$

Hence, the two-parameter group G , which invariantly transforms Equations (21) and (22), and the boundary condition (23) takes the form

$$G : \begin{cases} \bar{x} = x + K^x(a_1, a_2) \\ \bar{r} = r \\ \bar{t} = t + K^t(a_1, a_2) \\ \bar{\psi} = \psi + K^\psi(a_1, a_2) \\ \bar{\theta} = \theta \\ \bar{H} = H \end{cases}. \quad (39)$$

3.3. The Complete Set of Absolute Invariants

The basic tool of this technique is the application of a general theorem from group theory, so that the problem under consideration is described by ODEs (similarity representation) in an independent variable (similarity variable). Herein, the complete sets of absolute invariants include two types of absolute invariants, namely (i) the absolute invariants of independent variables (x, r, t) , which are $\eta = \eta(x, r, t)$, and (ii) the absolute invariants of dependent variables (ψ, θ, H) . This general theorem for the case of a two-parameter group (e.g., [54,55]), states that a function $\eta = \eta(x, r, t)$ is an absolute invariant of a two-parameter group of the form

$$\bar{S} : \begin{aligned} \bar{x} &= C^x(a_1, a_2) x + K^x(a_1, a_2), \\ \bar{r} &= C^r(a_1, a_2) r + K^r(a_1, a_2), \\ \bar{t} &= C^t(a_1, a_2) t + K^t(a_1, a_2). \end{aligned} \quad (40)$$

If and only if η satisfies the first order linear PDEs:

$$\begin{aligned} (\alpha_1 x + \alpha_2) \frac{\partial \eta}{\partial x} + (\alpha_3 r + \alpha_4) \frac{\partial \eta}{\partial r} + (\alpha_5 t + \alpha_6) \frac{\partial \eta}{\partial t} &= 0, \\ (\delta_1 x + \delta_2) \frac{\partial \eta}{\partial x} + (\delta_3 r + \delta_4) \frac{\partial \eta}{\partial r} + (\delta_5 t + \delta_6) \frac{\partial \eta}{\partial t} &= 0, \end{aligned} \quad (41)$$

where

$$\begin{aligned} \alpha_1 &= \frac{\partial C^x}{\partial a_1} (a_1^0, a_2^0), \alpha_2 = \frac{\partial K^x}{\partial a_1} (a_1^0, a_2^0), \alpha_3 = \frac{\partial C^r}{\partial a_1} (a_1^0, a_2^0), \alpha_4 = \frac{\partial K^r}{\partial a_1} (a_1^0, a_2^0), \\ \alpha_5 &= \frac{\partial C^t}{\partial a_1} (a_1^0, a_2^0), \alpha_6 = \frac{\partial K^t}{\partial a_1} (a_1^0, a_2^0), \delta_1 = \frac{\partial C^x}{\partial a_2} (a_1^0, a_2^0), \delta_2 = \frac{\partial K^x}{\partial a_2} (a_1^0, a_2^0), \\ \delta_3 &= \frac{\partial C^r}{\partial a_2} (a_1^0, a_2^0), \delta_4 = \frac{\partial K^r}{\partial a_2} (a_1^0, a_2^0), \delta_5 = \frac{\partial C^t}{\partial a_2} (a_1^0, a_2^0), \delta_6 = \frac{\partial K^t}{\partial a_2} (a_1^0, a_2^0). \end{aligned}$$

and (a_1^0, a_2^0) denote the values of a_1 and a_2 , which yield the identity: $\bar{x} = x, \bar{r} = r, \bar{t} = t$ according to [55]. By definition, there is one functionally independent solution to (41). Additionally, if η is a non-constant solution to (41) for a group S , then every other solution

to (41), for S , is given in the form $J(\eta)$ where J is a differentiable function. From (41) and the definitions of the constants α_i, δ_i , it can be seen that distinctions between group S are reflected by the α' s and δ' s. This means that, in general, any particular group S owns a characteristic set of α' s and δ' s and, consequently, a characteristic absolute invariant η is yielded by (41).

Since $K^r \equiv 0$, it is $\alpha_4 = \delta_4 = 0$ and Equation (41) becomes:

$$\begin{aligned} (\alpha_1 x + \alpha_2) \frac{\partial \eta}{\partial x} + \alpha_3 r \frac{\partial \eta}{\partial r} + (\alpha_5 t + \alpha_6) \frac{\partial \eta}{\partial t} &= 0, \\ (\delta_1 x + \delta_2) \frac{\partial \eta}{\partial x} + \delta_3 r \frac{\partial \eta}{\partial r} + (\delta_5 t + \delta_6) \frac{\partial \eta}{\partial t} &= 0. \end{aligned} \quad (42)$$

4. Derivation of Distinct Complete Sets

In this section, the distinct complete sets of invariants will be derived.

Invariants for the independent variables

As already mentioned in the previous section, system (42) has one functionally independent solution, which means that the rank of the coefficient matrix for $\left\{ \frac{\partial \eta}{\partial x}, \frac{\partial \eta}{\partial r}, \frac{\partial \eta}{\partial t} \right\}$ must be two. This is true whenever at least one of the following conditions is satisfied:

$$\lambda_{31}x + \lambda_{32} \neq 0 \text{ or } \lambda_{35}t + \lambda_{36} \neq 0 \text{ or } \lambda_{15}xt + \lambda_{16}x + \lambda_{25}t + \lambda_{26} \neq 0, \quad (43)$$

where

$$\lambda_{ij} = \alpha_i \delta_j - \alpha_j \delta_i, \quad i, j = 1, 2, 3, 4, 5, 6$$

and it should be mentioned that from the definitions of α' s, δ' s and λ' s, as well as from the transformations (39), it can be found that:

$$\lambda_{31} = \lambda_{35} = \lambda_{15} = 0. \quad (44)$$

For convenience, (42) can be rewritten in terms of (43) in the form:

$$\begin{aligned} (\lambda_{31}x + \lambda_{32}) \frac{\partial \eta}{\partial x} + (\lambda_{35}t + \lambda_{36}) \frac{\partial \eta}{\partial t} &= 0, \\ (\lambda_{31}x + \lambda_{32}) r \frac{\partial \eta}{\partial r} - (\lambda_{15}xt + \lambda_{16}x + \lambda_{25}t + \lambda_{26}) \frac{\partial \eta}{\partial t} &= 0. \end{aligned} \quad (45)$$

According to conditions (43), three main cases arise which will be studied in the following:

4.1. First Case: None of the Coefficients in (45) Vanish Identically

Assume that

$$\lambda_{31}x + \lambda_{32} \neq 0 \text{ and } \lambda_{35}t + \lambda_{36} \neq 0 \text{ and } \lambda_{15}xt + \lambda_{16}x + \lambda_{25}t + \lambda_{26} \neq 0,$$

or taking into consideration (44) that

$$\lambda_{32} \neq 0 \text{ and } \lambda_{36} \neq 0 \text{ and } \lambda_{16}x + \lambda_{25}t + \lambda_{26} \neq 0. \quad (46)$$

In this case, (45) becomes

$$\begin{aligned} \lambda_{32} \frac{\partial \eta}{\partial x} + \lambda_{36} \frac{\partial \eta}{\partial t} &= 0 \\ \lambda_{32} r \frac{\partial \eta}{\partial r} - (\lambda_{16}x + \lambda_{25}t + \lambda_{26}) \frac{\partial \eta}{\partial t} &= 0. \end{aligned} \quad (47)$$

According to a standard technique for linear PDEs, the first equation of (47) has the general solution

$$\eta = f(r, \xi(x, t)), \quad (48)$$

where f is an arbitrary function and ξ is a function such that

$$\xi(x, t) = \lambda_{36}x - \lambda_{32}t = c, \quad (49)$$

where c constant. Substitution of (48) to the second equation of (47) gives

$$r \frac{\partial \eta}{\partial r} - \frac{\lambda_{16}x + \lambda_{25}t + \lambda_{26}}{\lambda_{32}} \frac{\partial \xi}{\partial t} \frac{\partial f}{\partial \xi} = 0. \quad (50)$$

Since ξ is independent of r , the coefficient of $\frac{\partial f}{\partial \xi}$ in (50) must also be independent of r , i.e.,

$$\frac{\lambda_{16}x + \lambda_{25}t + \lambda_{26}}{\lambda_{32}} \frac{\partial \xi}{\partial t} = g(\xi),$$

which, after taking (49) into consideration, becomes

$$g(\xi) = -(\lambda_{16}x + \lambda_{25}t + \lambda_{26}) \quad (51)$$

However, since g is a function of only ξ , it is

$$\left. \frac{\partial g}{\partial x} \right|_{\xi} = \left. \frac{\partial g}{\partial x} \right|_t + \left. \frac{\partial g}{\partial t} \right|_x \left. \frac{\partial t}{\partial x} \right|_{\xi} \equiv 0,$$

which, after using (49) and (51), gives

$$-\lambda_{16} = -\lambda_{16} - \lambda_{25} \frac{\lambda_{36}}{\lambda_{36}} = 0 \Rightarrow \begin{cases} \lambda_{16} = 0 \\ \lambda_{16} + \lambda_{25} \frac{\lambda_{36}}{\lambda_{36}} = 0 \end{cases} \Rightarrow \begin{cases} \lambda_{16} = 0 \\ \lambda_{25} = 0 \end{cases},$$

after taking (46) into consideration. However, due to the definitions of α 's, δ 's and λ 's, as well as from the transformations (39), it is $\alpha_1 = \alpha_3$ and $\delta_1 = \delta_3$. Thus,

$$\lambda_{16} = 0 \Rightarrow \alpha_1 \delta_6 - \alpha_6 \delta_1 = 0 \Rightarrow \alpha_3 \delta_6 - \alpha_6 \delta_3 = 0 \Rightarrow \lambda_{36} = 0,$$

which contradicts the second assumption of (46). Consequently, this first case is not acceptable.

4.2. Second Case: Two of the Coefficients in (45) Vanish Identically

Sub-case 2-I: Assume that

$$\lambda_{31}x + \lambda_{32} \equiv 0, \lambda_{35}t + \lambda_{36} \equiv 0 \text{ and } \lambda_{15}xt + \lambda_{16}x + \lambda_{25}t + \lambda_{26} \neq 0.$$

In this case, (45) reduces to the following one equation

$$(\lambda_{15}xt + \lambda_{16}x + \lambda_{25}t + \lambda_{26}) \frac{\partial \eta}{\partial t} = 0,$$

since the first equation of (45) is identically satisfied, from which it is deduced that

$$\frac{\partial \eta}{\partial t} = 0. \quad (52)$$

By substituting (52) into (42) and after some manipulations, the following equations are obtained:

$$\left. \begin{aligned} (\lambda_{16}x + \lambda_{26}) \frac{\partial \eta}{\partial x} + \lambda_{36}r \frac{\partial \eta}{\partial r} &= 0 \\ (\lambda_{15}xt + \lambda_{25}t) \frac{\partial \eta}{\partial x} + \lambda_{35}rt \frac{\partial \eta}{\partial r} &= 0 \end{aligned} \right\},$$

which in turn yields the equation

$$(\lambda_{15}xt + \lambda_{16}x + \lambda_{25}t + \lambda_{26}) \frac{\partial \eta}{\partial x} + (\lambda_{35}t + \lambda_{36})r \frac{\partial \eta}{\partial r} = 0 \Rightarrow \quad (53)$$

$$\Rightarrow \frac{\partial \eta}{\partial x} = 0. \quad (54)$$

From (52) and (53), it is obvious that η is an arbitrary function of r alone, which for reasons of simplicity can be assumed to have the form

$$\eta = r \quad (55)$$

Sub-case 2-II: Assume that

$$\lambda_{31}x + \lambda_{32} \neq 0, \lambda_{35}t + \lambda_{36} \equiv 0 \text{ and } \lambda_{15}xt + \lambda_{16}x + \lambda_{25}t + \lambda_{26} \equiv 0.$$

In this case, (45) becomes

$$\left. \begin{array}{l} (\lambda_{31}x + \lambda_{32}) \frac{\partial \eta}{\partial x} = 0 \\ (\lambda_{31}x + \lambda_{32}) r \frac{\partial \eta}{\partial r} = 0 \end{array} \right\} \Rightarrow \left. \begin{array}{l} \frac{\partial \eta}{\partial x} = 0 \\ \frac{\partial \eta}{\partial r} = 0 \end{array} \right\},$$

from which it is deduced that η is not a function of r , which is unacceptable from the point of view of the boundary conditions.

Sub-case 2-III: Assume that

$$\lambda_{31}x + \lambda_{32} \equiv 0, \lambda_{35}t + \lambda_{36} \neq 0 \text{ and } \lambda_{15}xt + \lambda_{16}x + \lambda_{25}t + \lambda_{26} \equiv 0 \quad (56)$$

In this case, (45) reduces to the following one equation

$$(\lambda_{35}t + \lambda_{36}) \frac{\partial \eta}{\partial t} = 0,$$

since the first equation of (45) is identically satisfied, from which it is deduced that

$$\frac{\partial \eta}{\partial t} = 0.$$

Following the same procedure as in sub-case 2-I, Equation (53) appears, which due to (56) now gives

$$\frac{\partial \eta}{\partial r} = 0$$

Thus, η is not a function of r , which is unacceptable from the point of view of the boundary conditions.

4.3. Third Case: Only One of the Coefficients in (45) Vanishes Identically

Sub-case 3-I: Assume that

$$\lambda_{31}x + \lambda_{32} = 0, \lambda_{35}t + \lambda_{36} \neq 0, \lambda_{15}xt + \lambda_{16}x + \lambda_{25}t + \lambda_{26} \neq 0.$$

In this case, (45) reduces to the following one equation

$$\frac{\partial \eta}{\partial t} = 0,$$

which means that $\eta = \eta(x, r)$ and (42) is simplified to

$$\left. \begin{array}{l} (\alpha_1x + \alpha_2) \frac{\partial \eta}{\partial x} + \alpha_3r \frac{\partial \eta}{\partial r} = 0 \\ (\delta_1x + \delta_2) \frac{\partial \eta}{\partial x} + \delta_3r \frac{\partial \eta}{\partial r} = 0 \end{array} \right\},$$

a solution of which is found to be

$$\eta = r (Ax + B)^n, \quad (57)$$

where $n = -\frac{\alpha_3}{\alpha_1} = -\frac{\delta_3}{\delta_1}$, $A = \alpha_1 = \delta_1$, $B = \alpha_2 = \delta_2$.

Sub-case 3-II: Assume that

$$\lambda_{31}x + \lambda_{32} \neq 0, \quad \lambda_{35}t + \lambda_{36} = 0, \quad \lambda_{15}xt + \lambda_{16}x + \lambda_{25}t + \lambda_{26} \neq 0.$$

In this case, the first equation of (45) reduces to the following equation

$$(\lambda_{31}x + \lambda_{32}) \frac{\partial \eta}{\partial x} = 0 \Rightarrow \frac{\partial \eta}{\partial x} = 0,$$

which means that $\eta = \eta(r, t)$ and (42) is simplified to

$$\begin{aligned} \alpha_3 r \frac{\partial \eta}{\partial r} + (\alpha_5 t + \alpha_6) \frac{\partial \eta}{\partial t} &= 0, \\ \delta_3 r \frac{\partial \eta}{\partial r} + (\delta_5 t + \delta_6) \frac{\partial \eta}{\partial t} &= 0, \end{aligned}$$

a solution of which is found to be

$$\eta = r (Bt + A)^n, \quad (58)$$

where $n = \frac{\alpha_3}{\alpha_5} = \frac{\delta_3}{\delta_5}$, $A = \delta_6 = \alpha_6$, $B = \delta_5 = \alpha_5$.

Sub-case 3-III: Assume that

$$\lambda_{31}x + \lambda_{32} \neq 0, \quad \lambda_{35}t + \lambda_{36} \neq 0, \quad \lambda_{15}xt + \lambda_{16}x + \lambda_{25}t + \lambda_{26} = 0.$$

In this case, the second equation of (45) reduces to the following equation

$$(\lambda_{31}x + \lambda_{32}) r \frac{\partial \eta}{\partial r} = 0 \Rightarrow \frac{\partial \eta}{\partial r} = 0,$$

from which it is deduced that η is not a function of r , which is unacceptable from the point of view of the boundary conditions.

Invariants for the dependent variables

The next step is to obtain the absolute invariants of the dependent variables ψ, H and θ . From (37), it is derived that θ is itself an absolute invariant. Thus,

$$X_1(x, r, t ; \theta) = \theta(\eta).$$

A function $X_2(x, t ; \psi)$ is said to be an absolute invariant of a two-parameter group only when it satisfies the following first order PDEs:

$$\begin{aligned} (\alpha_1 x + \alpha_2) \frac{\partial X_2}{\partial x} + (\alpha_3 t + \alpha_4) \frac{\partial X_2}{\partial t} + (\alpha_5 \psi + \alpha_6) \frac{\partial X_2}{\partial \psi} &= 0 \\ (\delta_1 x + \delta_2) \frac{\partial X_2}{\partial x} + (\delta_3 t + \delta_4) \frac{\partial X_2}{\partial t} + (\delta_5 \psi + \delta_6) \frac{\partial X_2}{\partial \psi} &= 0, \end{aligned}$$

a solution of which is

$$X_2(x, t ; \psi) = \varphi_1 \left(\frac{\psi}{\Gamma_1(x, t)} \right) = F(\eta). \quad (59)$$

In a similar way, the following is found

$$X_3(x, t ; H) = \varphi_2 \left(\frac{H}{\Gamma_2(x, t)} \right) = E(\eta) \quad (60)$$

In (59)–(60), the functions $\Gamma_1(x, t)$ and $\Gamma_2(x, t)$ are to be determined so that eventually the PDEs (21)–(22) are reduced to ODEs. Without loss of generality, the functions φ_1 and φ_2 in (59)–(60), can be selected as the identity functions. Therefore, the functions $\psi(x, r, t)$ and $H(x, t)$ can be rewritten in terms of $F(\eta)$ and $E(\eta)$ in the following way:

$$\psi(x, r, t) = \Gamma_1(x, t)F(\eta), \quad H(x, t) = \Gamma_2(x, t)E(\eta). \quad (61)$$

Since $\Gamma_2(x, t)$ and $H(x, t)$ are independent of r and η depends on r , E must be a constant, say E_0 . Thus

$$\psi(x, r, t) = \Gamma_1(x, t)F(\eta), \quad H(x, t) = E_0\Gamma_2(x, t). \quad (62)$$

5. The Reduction to Ordinary Differential Equations

Assume that $\eta = r\pi(x, t)$. Using (62), the PDEs (21)–(22) and the boundary conditions (23) are reduced to the following system of ODEs:

$$r^2 F''' - C_1 r F'' + C_2 F' - C_3 A_2 r^2 M n F' + C_4 A_3 \beta r^3 \theta - A_1 [C_5 r^2 F' + C_6 r^3 F'' + C_7 r^2 F' + 2 C_8 r F'^2 - (r F F'' - r F'^2) C_9 + C_{10} F F'] = 0 \quad (63)$$

$$(1 + N r A_5) r \theta'' + C_1 \theta' - A_4 \text{Pr} [C_6 r^2 \theta' - C_9 F \theta'] - C_{11} A_5 \beta E c (\varepsilon - \theta) F' = 0, \quad (64)$$

with corresponding boundary conditions

$$\begin{aligned} r = 1 : & F = 0, F' = 0, \theta = 1, \\ r \rightarrow \infty : & F' = 0, \theta = 0. \end{aligned} \quad (65)$$

where

$$\begin{aligned} C_1 &= \frac{1}{\pi}, C_2 = \frac{1}{\pi^2}, C_3 = \frac{\Gamma_2^2 E_0^2}{\pi^2}, C_4 = \frac{\Gamma_2 E_0^2}{\Gamma_1 \pi^3} \frac{\partial \Gamma_2}{\partial x}, C_5 = \frac{1}{\pi^3} \frac{\partial \pi}{\partial t}, C_6 = \frac{1}{\pi^2} \frac{\partial \pi}{\partial t}, \\ C_7 &= \frac{1}{\Gamma_1 \pi^2} \frac{\partial \Gamma_1}{\partial t}, C_8 = \frac{\Gamma_1}{\pi^2} \frac{\partial \pi}{\partial x}, C_9 = \frac{1}{\pi} \frac{\partial \Gamma_1}{\partial x}, C_{10} = \frac{1}{\pi^2} \frac{\partial \Gamma_1}{\partial x}, C_{11} = \frac{\Gamma_1 \Gamma_2 E_0^2}{\pi} \frac{\partial \Gamma_2}{\partial x}. \end{aligned} \quad (66)$$

The C 's defined in (66) are constants to be determined for every individual case corresponding to every set of absolute invariants. For this, the following three cases are considered:

Case (a)

Consider $\eta = r\pi(x, t)$ as in (55), i.e., $\pi(x, t) = 1$ and $\Gamma_1 = \Gamma_1(x), \Gamma_2 = \Gamma_2(x)$. In this case and by further assuming C_3 to be unity, (66) gives

$$\begin{aligned} C_1 &= C_2 = C_3 = 1, C_9 = C_{10}, C_5 = C_6 = C_7 = C_8 = 0, C_4 = \frac{C_{11}}{\Gamma_1^2}, \\ \Gamma_1 &= C_9 x + K_1 = C_{10} x + K_2, \Gamma_2 = K_3 (C_9 x + K_1)^{\frac{C_{11}}{C_9}} = K_3 (C_{10} x + K_2)^{\frac{C_{11}}{C_{10}}}, \end{aligned}$$

where K_1, K_2, K_3 are constants of integration. Substitution of the aforementioned values into (63)–(64), gives:

$$r^2 F''' - r F'' + F' - A_2 r^2 M n F' - A_1 \left((r F'^2 - r F F'') C_9 + C_9 F F' \right) + C_4 A_3 \beta r^3 \theta = 0, \quad (67)$$

$$(1 + N r A_5) r \theta'' + \theta' + A_4 C_9 \text{Pr} F \theta' - C_{11} A_5 \beta E c (\varepsilon - \theta) F' = 0. \quad (68)$$

Equations (67)–(68) are accompanied of course by the boundary conditions (65), i.e.:

$$\begin{aligned} r = 1 : & F = 0, F' = 0, \theta = 1, \\ r \rightarrow \infty : & F' = 0, \theta = 0. \end{aligned} \quad (69)$$

In this case, the functions ψ and H given by (62) take the form

$$\begin{aligned} \psi &= (C_9 x + K_1) F(\eta) = (C_{10} x + K_2) F(\eta), \\ H &= K_3 (C_9 x + K_1)^{\frac{C_{11}}{C_9}} E_0 = K_3 (C_{10} x + K_2)^{\frac{C_{11}}{C_{10}}} E_0, \end{aligned} \quad (70)$$

and the corresponding velocity components are:

$$\begin{aligned} u &= \frac{1}{r} \frac{\partial \psi}{\partial r} = (C_9 x + K_1) \frac{\pi}{r} F' = (C_{10} x + K_2) \frac{\pi}{r} F', \\ v &= -\frac{1}{r} \frac{\partial \psi}{\partial x} = -\frac{C_9}{r} F = -\frac{C_{10}}{r} F. \end{aligned} \quad (71)$$

Case (b)

Consider $\eta = r\pi(x, t)$ as in (57), i.e., $\pi(x, t) = (Ax + B)^n$ and $\Gamma_1 = \Gamma_1(x), \Gamma_2 = \Gamma_2(x)$. In this case and by further assuming C_3 to be unity, (66) gives

$$\begin{aligned} C_1 &= \frac{1}{(Ax+B)^n}, C_2 = C_1^2, C_3 = 1, C_4 = \frac{An}{K}(Ax+B)^{-2n-2}, C_5 = C_6 = C_7 = 0, C_8 = AKn, \\ C_9 &= AK(n+1), C_{10} = \frac{AK(n+1)}{(Ax+B)^n}, C_{11} = AKn(Ax+B)^{2n}, \end{aligned}$$

where K is a constant of integration. Substitution of the aforementioned values into (63)–(64), gives:

$$\begin{aligned} r^2F''' - C_1rF'' + C_1^2F' - A_2r^2MnF' + C_4A_3\beta r^3\theta \\ - A_1[2C_8rF'^2 - (rFF'' - rF'^2)C_9 + C_{10}FF'] = 0 \end{aligned} \quad (72)$$

$$(1 + NrA_5)r\theta'' + C_1\theta' + A_4C_9PrF\theta' - C_{11}A_5\beta Ec(\varepsilon - \theta)F' = 0. \quad (73)$$

Equations (72)–(73) are accompanied of course by the boundary conditions (65), i.e.:

$$\begin{aligned} r = 1 : F = 0, F' = 0, \theta = 1, \\ r \rightarrow \infty : F' = 0, \theta = 0. \end{aligned} \quad (74)$$

In this case, the functions ψ and H given by (62) take the form

$$\begin{aligned} \psi &= K(Ax + B)^{n+1}F, \\ H &= (Ax + B)^n, \end{aligned} \quad (75)$$

and the corresponding velocity components are:

$$\begin{aligned} u &= \frac{1}{r}\frac{\partial\psi}{\partial r} = \frac{K}{r}(Ax + B)^{2n+1}F', \\ v &= -\frac{1}{r}\frac{\partial\psi}{\partial x} = -\Gamma_1An(Ax + B)^{n-1}F' - \frac{K}{r}A(n+1)(Ax + B)^nF. \end{aligned} \quad (76)$$

Case (c)

Consider $\eta = r\pi(x, t)$ as in (58), i.e., where $\pi(x, t) = (Bt + A)^n$ for $n = -\frac{1}{2}$ and $\Gamma_1 = \Gamma_1(x, t), \Gamma_2 = \Gamma_2(x, t)$. In this case and by further assuming C_3 to be unity, (66) gives

$$\begin{aligned} C_1 &= \sqrt{Bt+A}, C_2 = Bt + A, C_3 = 1, C_4 = C_8 = C_{11} = 0, C_5 = -\frac{B}{2}, C_6 = -\frac{B}{2C_1}, \\ C_7 &= -\frac{B}{2}, C_{10} = C_1C_9. \end{aligned}$$

Substitution of the aforementioned values into (63)–(64), gives:

$$\begin{aligned} r^2F''' - C_1rF'' + C_2F' - A_2r^2MnF' - A_1[-\frac{B}{2}r^2F' - \frac{B}{2}\eta r^2F'' - C_7r^2F' \\ + C_9C_1FF' - C_9(rFF'' - rF'^2)] = 0, \end{aligned} \quad (77)$$

$$(1 + NrA_5)r\theta'' + C_1\theta' + A_4Pr\left[\frac{B}{2}\eta r\theta' - C_9F\theta'\right] = 0. \quad (78)$$

Equations (77)–(78) are accompanied of course by the boundary conditions (65), i.e.:

$$\begin{aligned} r = 1 : F = 0, F' = 0, \theta = 1, \\ r \rightarrow \infty : F' = 0, \theta = 0. \end{aligned} \quad (79)$$

In this case, the functions ψ and H given by (62) take the form

$$\begin{aligned} \psi &= \frac{(x+K_1)}{\sqrt{Bt+A}}C_9F, \\ H &= \frac{1}{\sqrt{Bt+A}}, \end{aligned} \quad (80)$$

where K_1 is a constant of integration, and the corresponding velocity components are:

$$\begin{aligned} u &= \frac{1}{r} \frac{\partial \psi}{\partial r} = \frac{(x+K_1)}{(Bt+A)r} C_9 F' , \\ v &= -\frac{1}{r} \frac{\partial \psi}{\partial x} = -\frac{C_9}{r\sqrt{(Bt+A)}} . \end{aligned} \quad (81)$$

It can be observed, that cases (a) and (b) the impacts of the ferromagnetic number and the magnetic field parameter in velocity and temperature profiles are significant compared to case (c), since, in case (c), the FHD parameter is absent. For these reasons, only cases (a) and (b) are numerically solved.

6. The Numerical Procedure

To numerically solve the fluid mechanics problem described by equations such as (63)–(65), several computational techniques have been proposed by many researchers. In this paper, an efficient numerical technique is employed based on the common finite differences method with central differencing, a tridiagonal matrix manipulation and an iterative procedure introduced in [56]. In this section, this technique will be described for case (b). First of all, the arbitrary coefficient constants in (72)–(73) are for reasons of simplicity, all assumed to be equal to one. Therefore, (72)–(73) are rewritten as:

$$r^2 F''' - rF'' + F' - A_2 r^2 M n F' + A_3 \beta r^3 \theta - A_1 \left[2rF'^2 - (rFF'' - rF'^2) + FF' \right] = 0, \quad (82)$$

$$(1 + NrA_5) r\theta'' + \theta' + A_4 \text{Pr}F\theta' - A_5 \beta Ec (\varepsilon - \theta) F' = 0. \quad (83)$$

Following [49], Equation (82) is written in the form

$$r^2 F''' + (A_1 rF - r) F'' + \left(1 - A_2 r^2 M - 2A_1 rF' - A_1 rF' - A_1 F \right) F' = -A_3 \beta r^3 \theta, \quad (84)$$

or

$$r^2 (F')'' + (A_1 rF - r) (F')' + \left(1 - A_2 r^2 M n - 2A_1 rF' - A_1 rF' - A_1 F \right) F' = -A_3 \beta r^3 \theta, \quad (85)$$

and (83) in the form

$$(1 + NrA_5) r\theta'' + (1 + A_4 \text{Pr}F)\theta' + A_5 \beta EcF'\theta = A_5 \beta Ec \varepsilon F'. \quad (86)$$

Both (85) and (86) are of the general form

$$Pg''(\eta) + Qg'(\eta) + Rg(\eta) = S \quad (87)$$

with

$$g = F'(\eta), P = r^2, Q = A_1 rF - r, R = 1 - A_2 r^2 M n - 2A_1 rF' - A_1 rF' - A_1 F, S = -A_3 \beta r^3 \theta,$$

or Equation (85) and

$$g = \theta(\eta), P = (1 + NrA_5) r, Q = 1 + A_4 \text{Pr}F, R = A_5 \beta EcF', S = A_5 \beta Ec \varepsilon F'$$

for Equation (86).

Equations (85)–(86) are solved by a common finite differences method based on central differencing and tridiagonal matrix manipulation. Before starting the solution procedure, it is necessary to assume an initial guess for $F'(\eta)$ and $\theta(\eta)$ between $\eta = 0$ and $\eta = \eta_\infty$ ($\eta \rightarrow \infty$) which satisfies the boundary conditions (74). Thus, it is assumed that

$$F(\eta) = \frac{\eta}{\eta_\infty}, \quad F'(\eta) = \frac{\eta}{\eta_\infty}, \quad \theta(\eta) = 1 - \frac{\eta}{\eta_\infty},$$

Therefore, the $F(\eta)$ distribution is obtained by integrating $F'(\eta)$. The function $\theta(\eta)$ is retained while a new estimation for $F'(\eta)$, say (F'_{new}), is determined by solving

(85) using the same technique. Thus, the $F(\eta)$ profile is updated by integrating the new $F'(\eta)$. These new distributions $F(\eta)$ and $F'(\eta)$ are then used for new inputs, etc. In this way, Equation (85) and, consequently, (72) is iteratively solved until the required convergence up to a small quantity ε_1 is attained. The converged profile of $F(\eta)$ is used to solve (86), using the same finite differences method, but without iteration, producing a new approximation for $\theta(\eta)$. In this way, the temperature profile $\theta(\eta)$ is obtained until the convergence ε_1 is attained.

This numerical scheme is continued until the trial convergence of the solution is performed. The applied step size used in this paper for case (b) is $h = \Delta\eta = 0.01$ for $\eta_{\min} = 0$ and $\eta_{\max} = 7$. The solution is convergent with an approximation to $\varepsilon_1 = 10^{-3}$. For case (a), the same step size is considered, i.e., $h = \Delta\eta = 0.01$, but for $\eta_{\min} = 0$, $\eta_{\max} = 12$ and $\varepsilon_1 = 10^{-3}$. The arbitrary constants C_4, C_9, C_{10} appearing in case (a) are also considered equal to one.

7. Results and Discussion

Before proceeding to the application of the above-mentioned method for the derivation of the numerical results, it is essential to check the accuracy of the applied numerical algorithm. For that, calculations were performed for partial cases of the present problem in order to perform comparisons with previously published results. For demonstration purposes, a graphical comparison is given in Figures 2 and 3 concerning results comparison obtained for the present case (b) with that obtained in [37] for the velocity and temperature distributions, respectively. From the relative figures as well as from all other comparisons performed, we found that the results are accurate and ensure the acceptability of the proposed numerical algorithm.

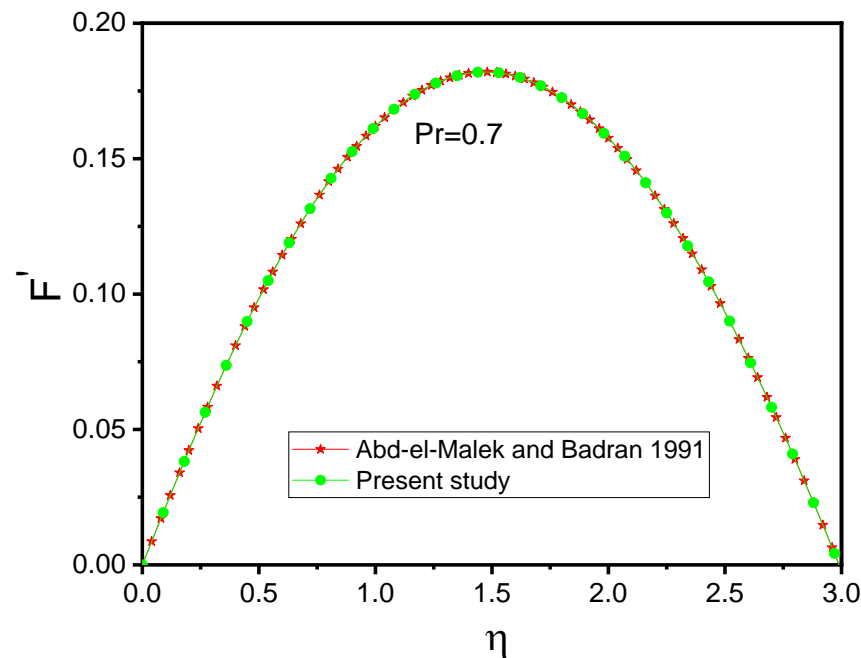


Figure 2. Comparison with [37] of F' for $Pr = 0.7$ with $\beta = Mn = Ec = Nr = \phi = 0$.

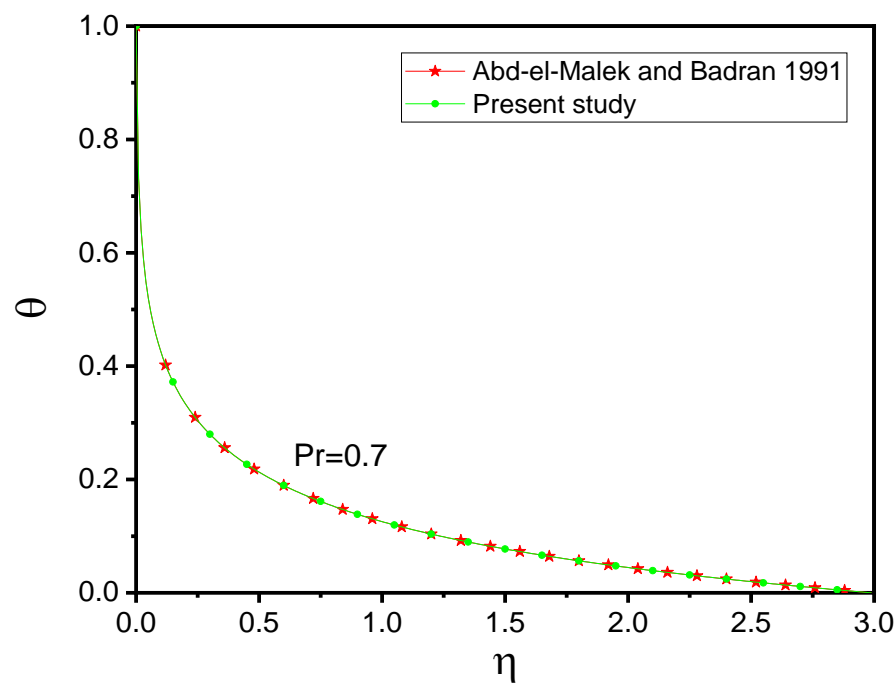


Figure 3. Comparison with [37] of θ for $Pr = 0.7$ with $\beta = Mn = Ec = Nr = \phi = 0$.

In the following, the numerical results in conjunction with the appearing parameters are discussed with their respective outcomes for the velocity, temperature profiles as well as the skin friction coefficient and the rate of heat transfer for both cases (a) and (b). Before moving on to the numerical procedure, we need to ensure the allocation of some realistic values of the respective parameter to ensure that the obtained results of the proposed model will be as realistic as possible. The consideration of realistic case scenarios has been made for similar physical BFD problems and thus the following values of the parameters are utilized for case (a) and case (b) as follows:

- (i) The ferromagnetic interaction parameter $\beta = 0 - 10$ as in [12,13,39,40,49];
- (ii) The magnetic field parameter $Mn = 1, 3, 5$ as in [13,40,49,57];
- (iii) The Prandtl number $Pr = 21, 23, 25$ as in [13,40,49];
- (iv) The radiation parameter $Nr = 0.1, 0.2, 0.5, 1, 1.5, 3$ as in [57];
- (v) The Eckert number $Ec = 0.001, 0.002, 0.003, 0.01, 1$ as in [58];
- (vi) The volume fraction $\phi = 0, 0.05, 0.1, 0.2$ as in [49].

Moreover, human body temperature is considered as $T_w = 37^\circ\text{C}$ [13,41], and body Curie temperature as $T_c = 41^\circ\text{C}$. For these values, the dimensionless temperature is turned out to be $\varepsilon = \frac{T_c}{T_c - T_w} = \frac{314}{314 - 310} = 78.5$ [39,40]. Hence, the required values of the Prandtl number for human blood is $Pr = \frac{(\mu C_p)_f}{\kappa_f} = \frac{3.2 \times 10^{-3} \times 3.9 \times 10^3}{0.5} \approx 25$.

For case (a), the graphical results are obtained for pure blood and blood- Fe_3O_4 , where magnetic particles are assumed of cylindrical shape. In case (b), the effect of magnetic particle shape is compared for blood- Fe_3O_4 flow on a cylindrical surface.

Figures 4–7 present the typical profiles for the velocity and temperature for numerous values of the ferromagnetic interaction parameter. It is alluded that when the values of the ferromagnetic interaction parameter are increased, the velocity profile is reduced and, consequently, the temperature profile is also decreased. This is due to the presence of the Kelvin force which is also known as resistive force, and it appears because of the fluid polarization at the inflow region. Figures 4 and 5 show the behaviors of pure blood and blood- Fe_3O_4 and for that particular case, the magnetic particles are assumed as cylindrical. It is seen from those figures that when the magnetic particles are mixed with blood, blood velocity and temperature is slightly increased throughout to the boundary layer compared

to the case when pure blood is considered. The more profound reduction in the velocity with the increment of the applied magnetic field strength is depicted at Figure 6 for the case b. This reduction in the velocity is immense for η —greater than approximately 1.5. Analogous suppression of the temperature distributions with the increment of the magnetic field strength, i.e., as β increases, are also observed at Figure 7. It is also noticed from the aforementioned figures (see Figure 7) that if the particle shape is cylindrical, then the blood temperature is more significantly increased than when the spherical shape is adopted. It is noted that in these figures the above behavior concerns the effect of increasing polarization for a given electrical conductivity effect, i.e., steady Mn.

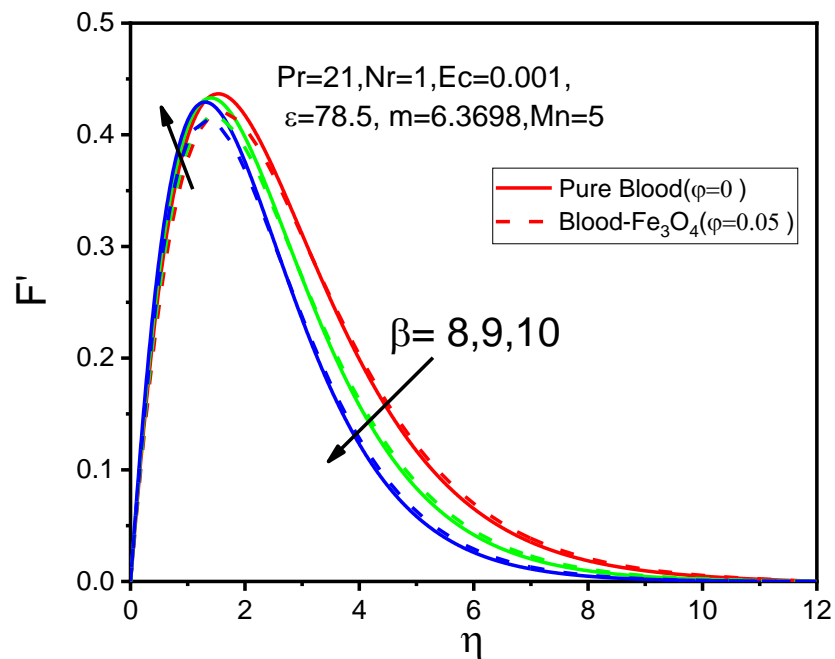


Figure 4. (Case a): Variations of F' for $\beta = 8, 9, 10$ against η .

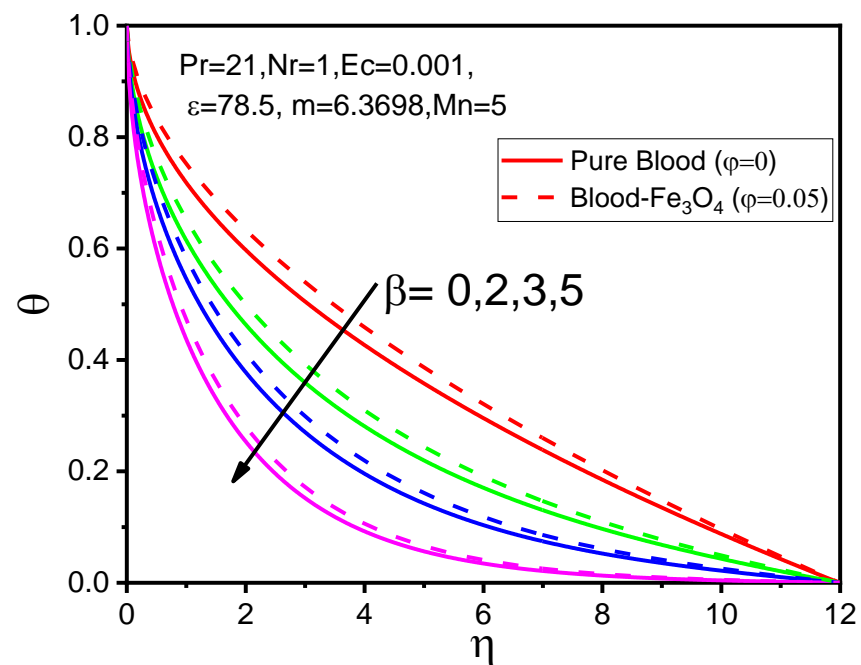


Figure 5. (Case a): Variations of θ for $\beta = 0, 2, 3, 5$ against η .

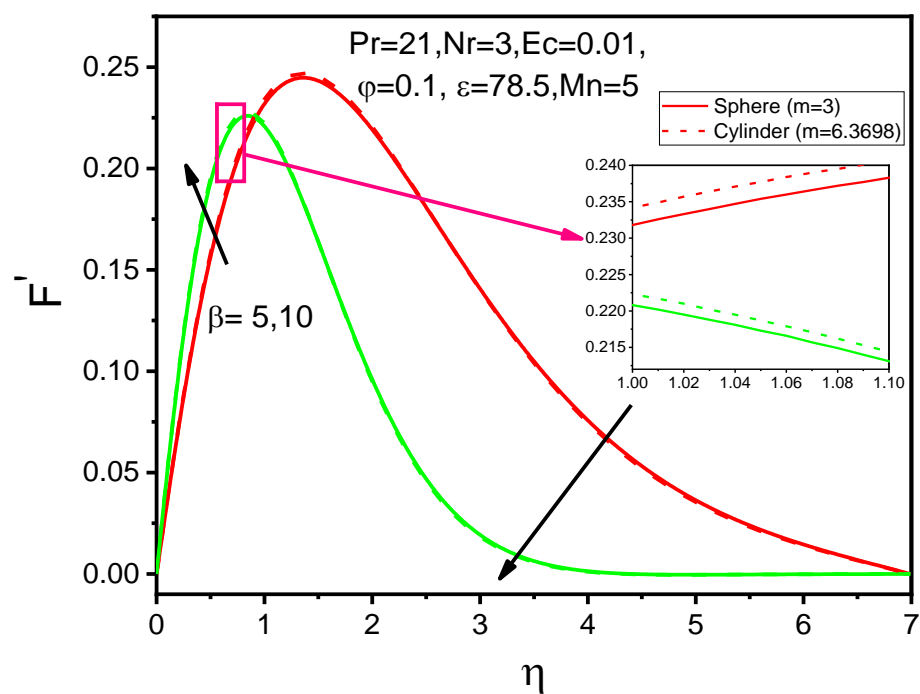


Figure 6. (Case b): Variations of F' for $\beta = 5, 10$ against η .

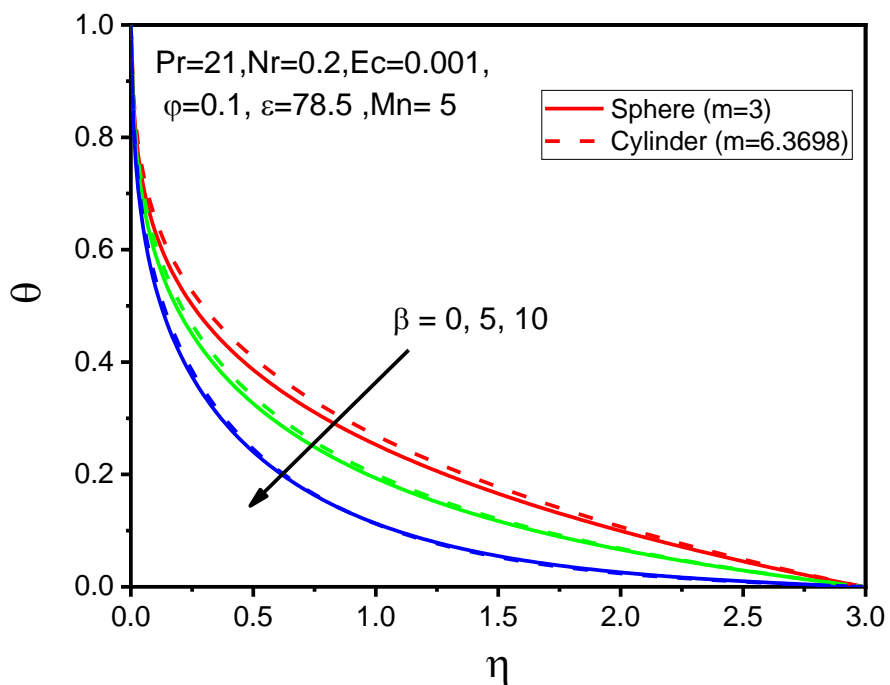


Figure 7. (Case b): Variations of θ for $\beta = 0, 5, 10$ against η .

The impact of the magnetic field parameter on the velocity and temperature distributions, for a steady ferromagnetic parameter β , are displayed in Figures 8 and 9. Figure 8 shows that blood velocity is decreased up to approximately $\eta \approx 1.9$ but then the fluid velocity is gradually increased. This is due to the application of the magnetic field which results to the arising of the Lorentz force, acting in the opposite direction to the fluid flow. As a result, for a given polarization effect, i.e., $\beta = 10$, when the values of the magnetic field parameter are increased, the temperature distribution is enhanced and that is clearly observed in Figure 9. A similar type of magnetic particle shape impact is also observed with

the variation of the magnetic field parameter and the ferromagnetic number. Additionally, from Figure 10, we found that the temperature of blood- Fe_3O_4 is much better enhanced after adding magnetic particles rather than that occurring for pure blood.

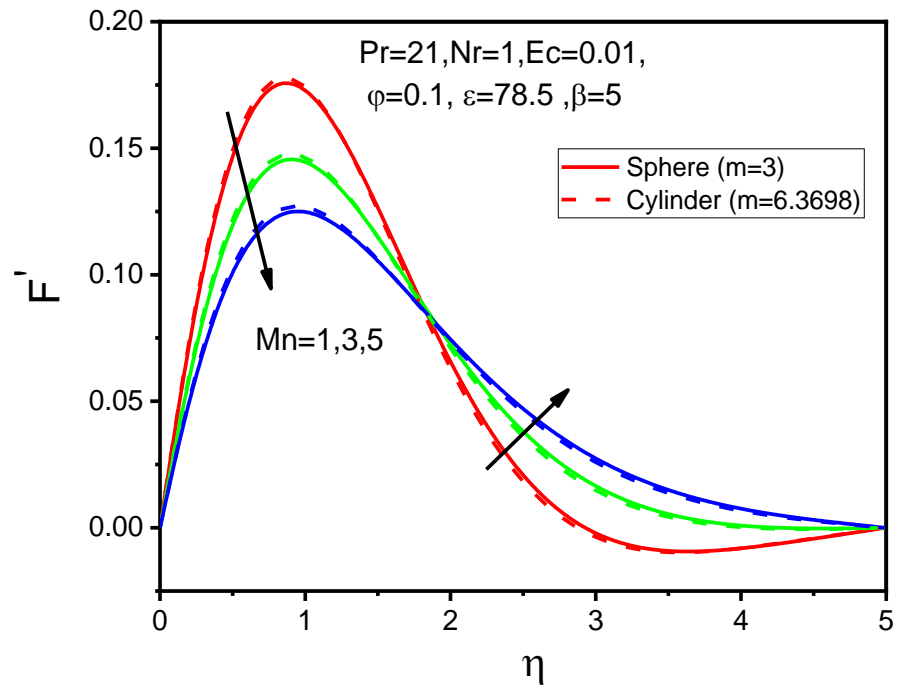


Figure 8. (Case b): Variations of F' for $Mn = 1, 3, 5$ against η .

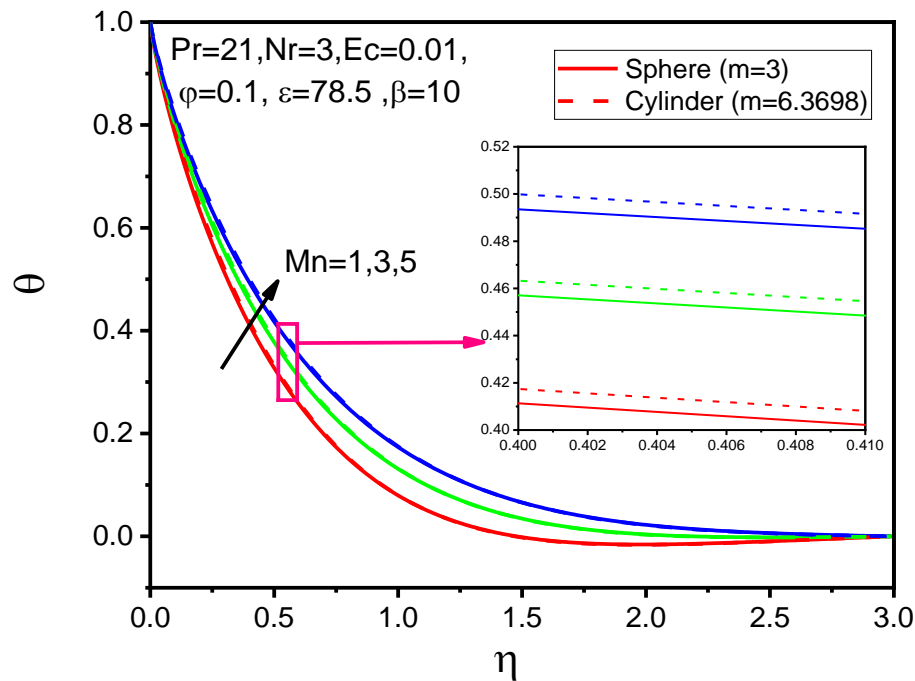


Figure 9. (Case b): Variations of θ for $Mn = 1, 3, 5$ against η .

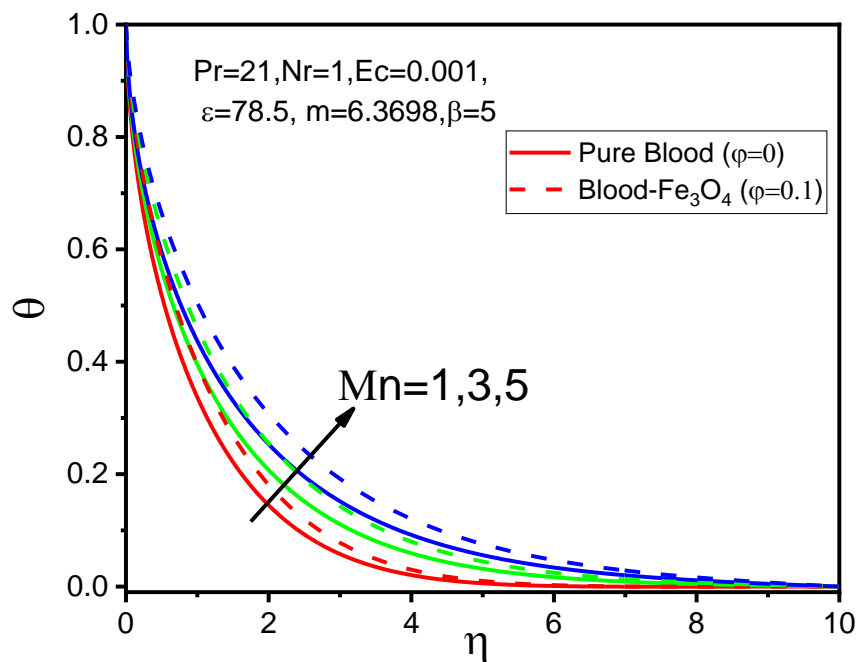


Figure 10. (Case a): Variations of θ for $Mn = 1, 3, 5$ against η .

Figures 11 and 12 present the effects of the magnetic particle volume fraction on the velocity and temperature profiles, respectively. It is evident that blood temperature is improved by the imposition of the magnetic particle volume fraction on blood (see Figure 12). It is also noticeable that it is more effective when particles are cylindrical rather than spherical. This is justified because of the large concentration of magnetic particles, which yields a higher proportion of thermal conductivity. From velocity profiles (Figure 11) two types of solutions are observed. Before the intersection of lines, it is observed that blood- Fe_3O_4 flow is decreased but after the intersection reverse trend is noticed as values of the magnetic particle volume fraction are enhanced. For both occasions, the magnetic particle shape factor plays a vital role, and their comparison is easily seen by observation of Figures 11 and 12.

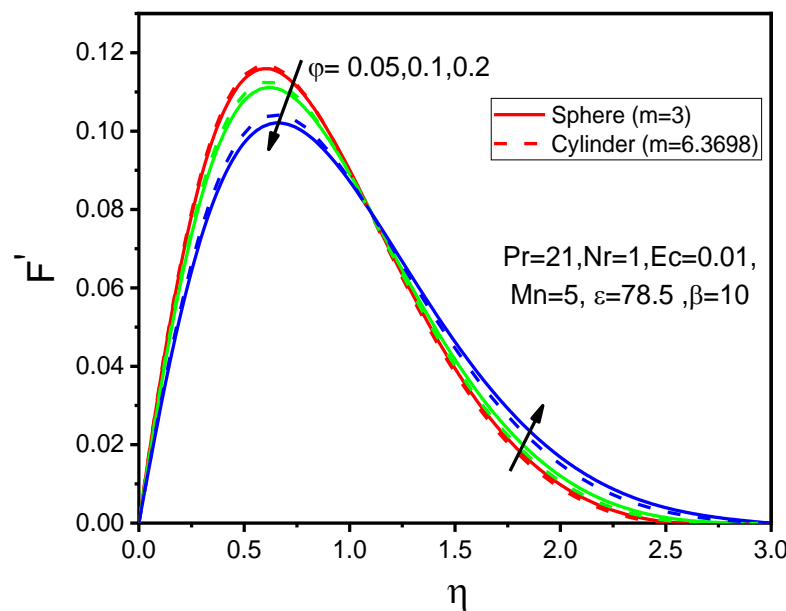


Figure 11. (Case b): Variations of F' for $\phi = 0.05, 0.1, 0.2$ against η .

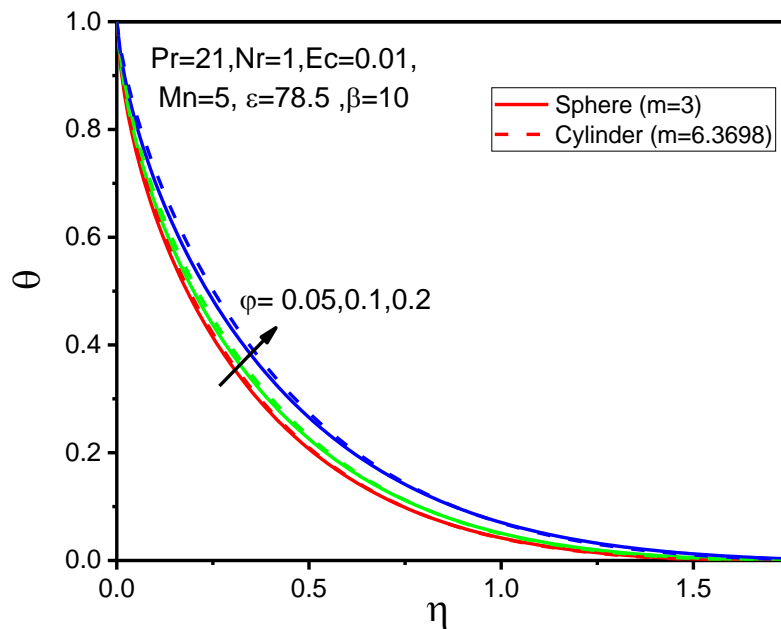


Figure 12. (Case b): Variations of θ for $\phi = 0.05, 0.1, 0.2$ against η .

The influence of the radiation parameter for various values on the velocity and temperature profiles, respectively, are plotted in Figures 13 and 14. From Figures 13 and 14, it is observed that, for a given magnetic field effect, i.e., Mn and β constants, as the values of the radiation parameter increase, both velocity and temperature distributions are increased. This is happening because heat energy is released from the fluid in the flow regime when the values of the radiation are gradually increased and as a result, the temperature of blood- Fe_3O_4 is enhanced.

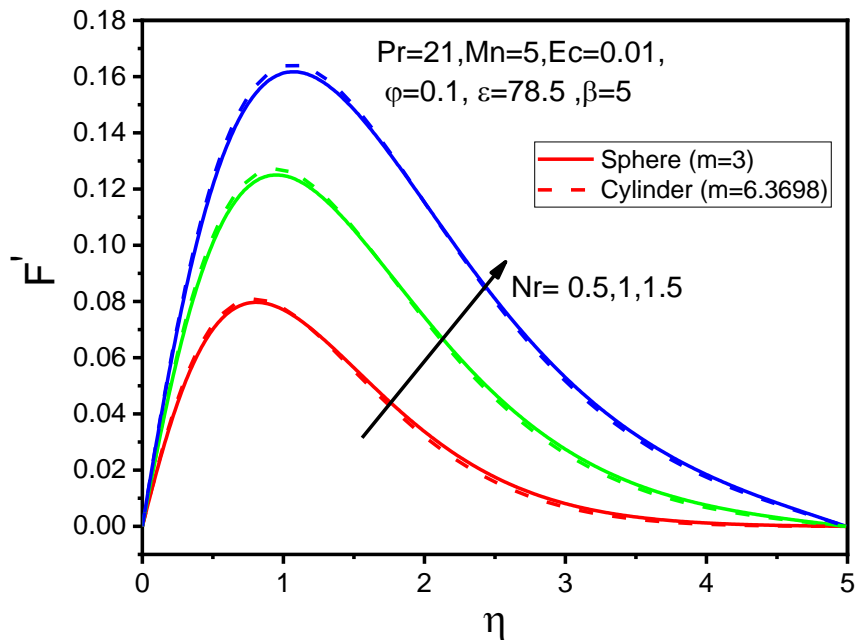


Figure 13. (Case b): Variations of F' for $Nr = 0.5, 1, 1.5$ against η .

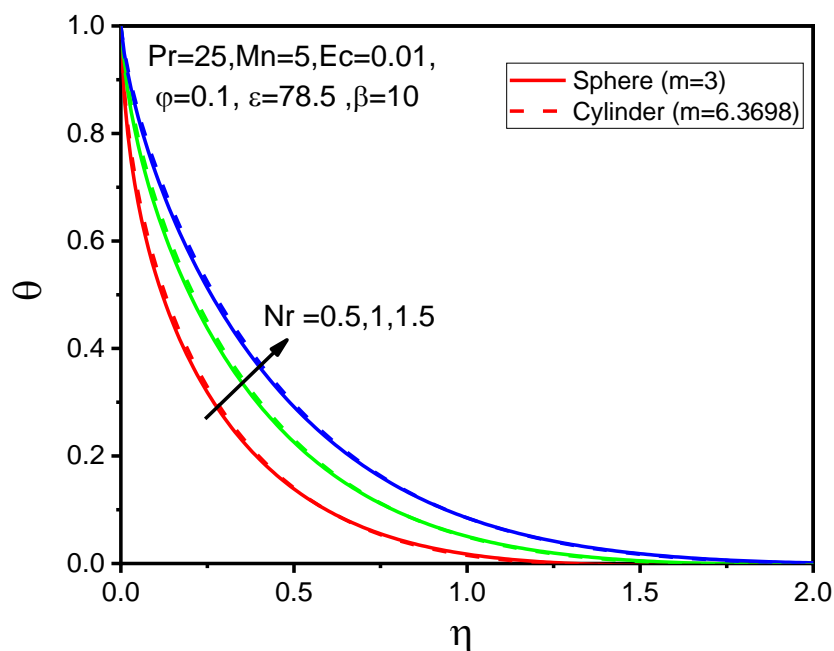


Figure 14. (Case b): Variations of θ for $Nr = 0.5, 1, 1.5$ against η .

Figures 15 and 16 represent the dimensionless velocity and temperature profiles, respectively, for various values of the Eckert number. As the Eckert number increases, both velocity and the temperature profiles are enhanced and especially the flow and heat of blood- Fe_3O_4 are remarkably increased compared to pure blood. Major temperature of fluid is attained for $Ec = 0.001$, which indicates that lower values of the Eckert number are responsible for enhancing temperature in fluid regime due to the combined effects of the magnetic field parameter and ferromagnetic number.

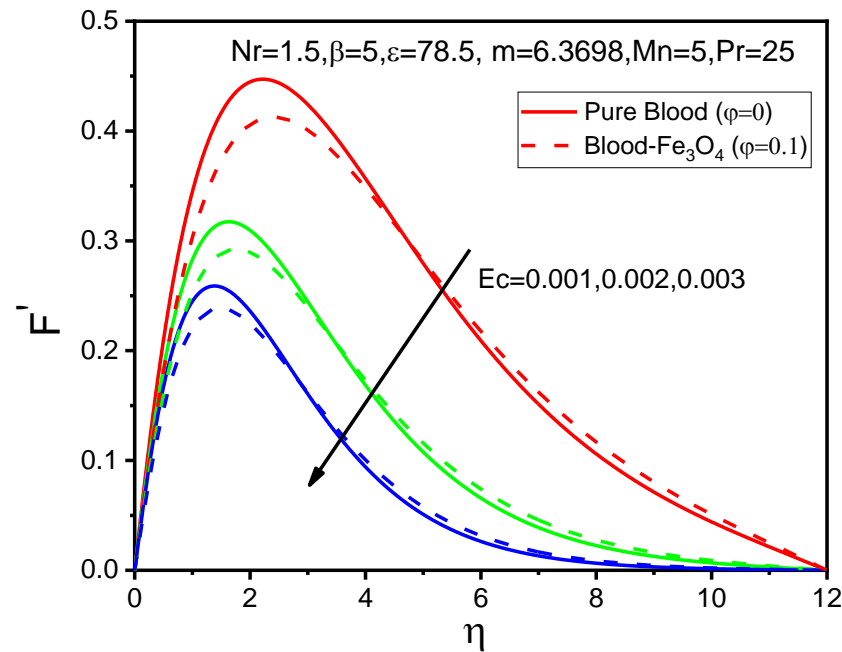


Figure 15. (Case a): Variations of F' for $Ec = 0.001, 0.002, 0.003$ against η .

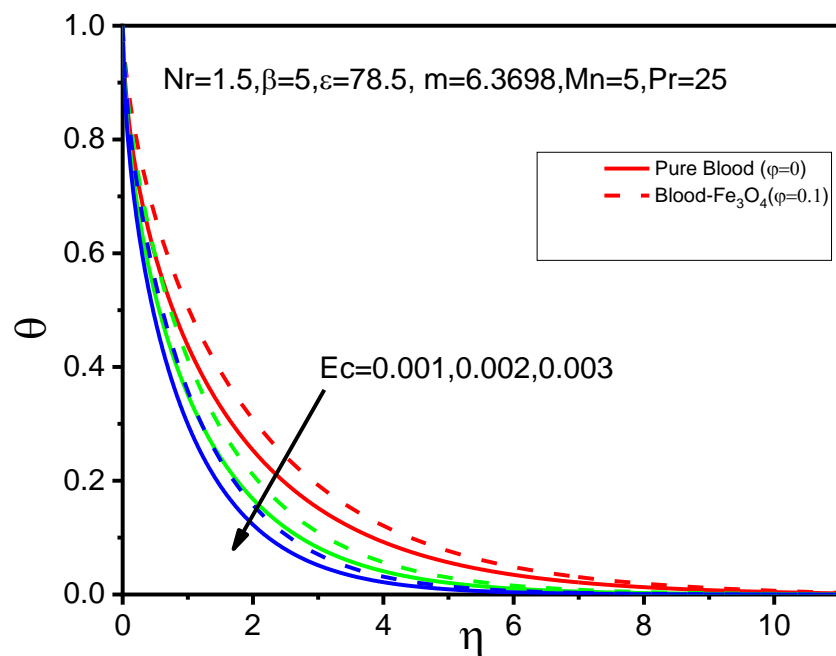


Figure 16. (Case a): Variations of θ for $Ec = 0.001, 0.002, 0.003$ against η .

Two quantities of great physical interest are the skin friction coefficient C_f and the rate of heat transfer Nu (local Nusselt number) which are defined by

$$C_f = \frac{2 \tau_w}{\rho_f \left(\frac{u_0 \bar{x}}{L} \right)^2}, \quad (88)$$

and

$$Nu = \frac{\bar{x} q_w}{\kappa_f (T_c - T_w)} \quad (89)$$

where $\tau_w = \mu_{mf} \left(\frac{\partial \bar{u}}{\partial \bar{r}} \right)_{\bar{r}=\bar{R}}$ is the wall shear stress parameter and $q_w = \kappa_{mf} \left(\frac{\partial \bar{T}}{\partial \bar{r}} \right)_{\bar{r}=\bar{R}}$ is the wall heat transfer parameter. Therefore, relations (88) and (89) take the following form:

$$C_f = \frac{2 \vartheta_f^2}{(1-\phi)^{2.5} \bar{R}^4 \left(\frac{u_0 x}{L} \right)^2} \left(\frac{\partial u}{\partial r} \right)_{r=1}, \quad (90)$$

and

$$Nu = - \frac{x \kappa_{mf}}{\kappa_f} \left(\frac{\partial \theta}{\partial r} \right)_{r=1}, \quad (91)$$

where $\vartheta_f^2 = \frac{\mu_f v_f}{\rho_f}$.

The skin friction coefficient and the local Nusselt number (the rate of heat transfer) are presented in Figures 17–22 for various values of the ferromagnetic interaction parameter, the magnetic particle volume fraction, the magnetic field parameter with regard to the magnetic field parameter, respectively. From Figures 17 and 18, we found that both the skin friction coefficient and the rate of heat transfer are increased for the ferromagnetic number with respect to the magnetic field parameter. It is noticeable from these figures that the rate of heat transfer of blood- Fe_3O_4 is significantly increased by approximately 33.2% compared to that of pure blood, whereas the reverse trend is observed in the skin friction coefficient and it is decreased by approximately 6.82% (see Figure 17). From Figure 19 to Figure 22, it is evident that both the skin friction coefficient and the Nusselt number are enhanced with the increment of the ferromagnetic interaction parameter, but the reverse trend is

observed from Figures 21 and 22 as the particle volume fraction is increased. However, it is also noticed that the skin friction coefficient of blood- Fe_3O_4 is effectively increased for the cylindrical shape of magnetic particles comparable to that of spherical shape and it is increased by approximately 1.09%, whereas the local Nusselt number of blood- Fe_3O_4 is reduced 0.08% for cylindrical shape than that of spherical shape.

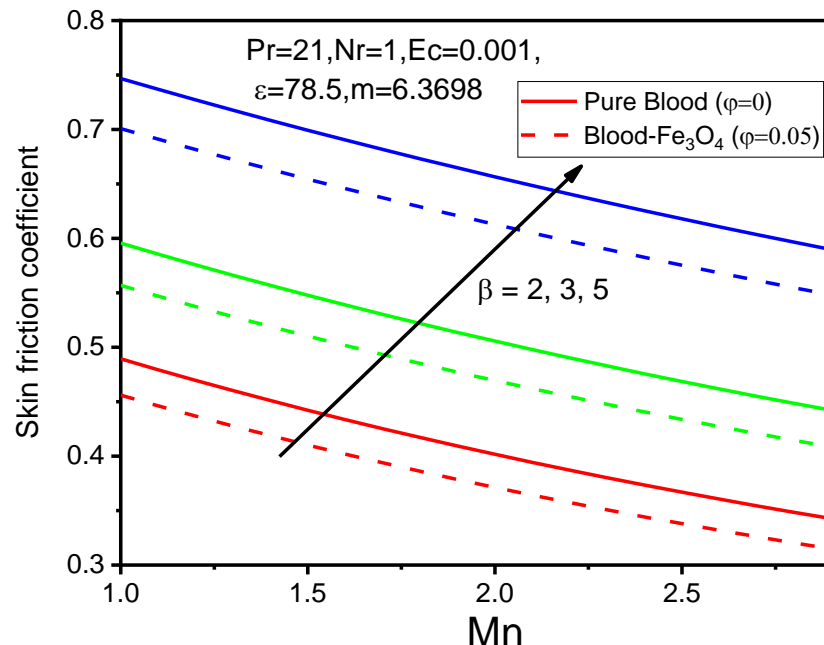


Figure 17. (Case a): Values of the skin friction coefficient for different values of β against Mn .

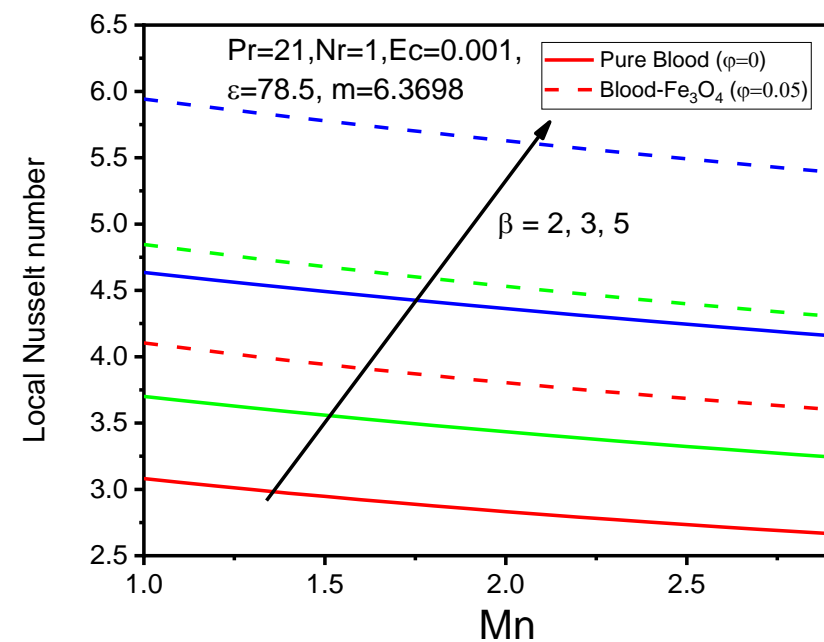


Figure 18. (Case a): Values of the local Nusselt number for different values of β against Mn .

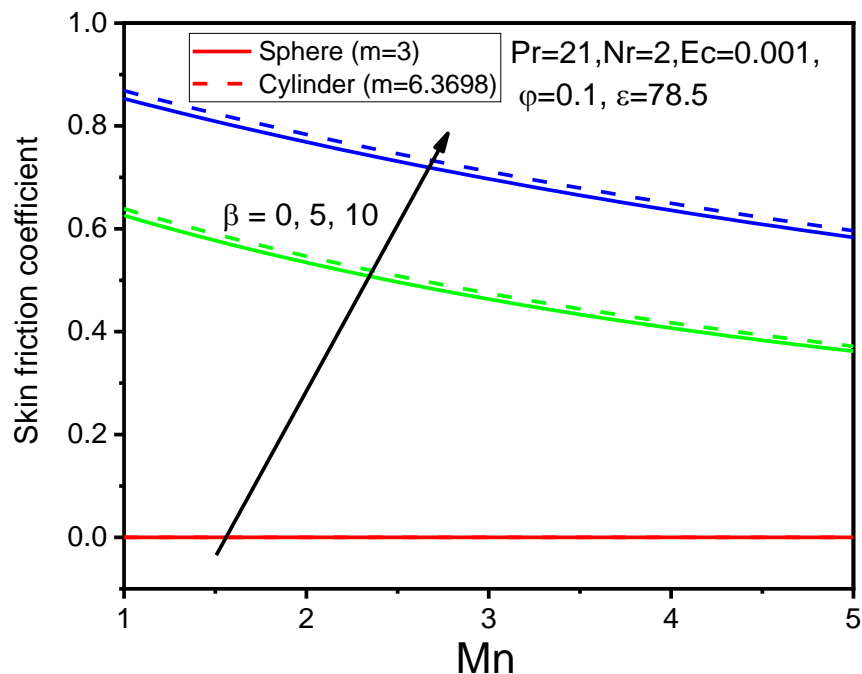


Figure 19. (Case b): Values of the skin friction coefficient for different values of β against Mn .

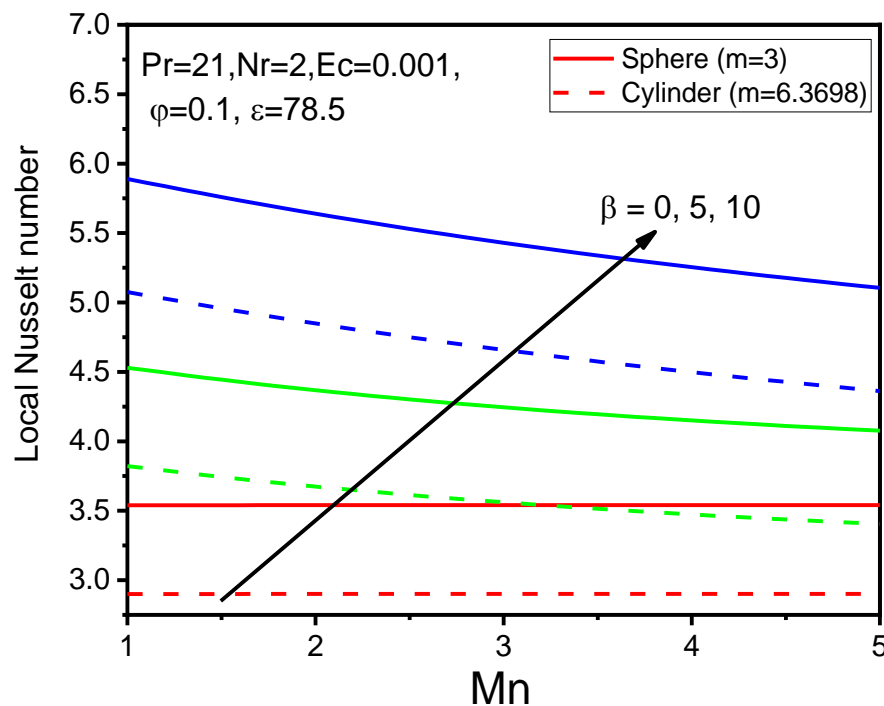


Figure 20. (Case b): Values of the local Nusselt number for different values of β against Mn .

For the ferromagnetic interaction parameter, the velocity profile is reduced and, consequently, the temperature profile is also decreased. This is due to the presence of the Kelvin force which is also known as resistive force, and it appears because of the fluid polarization at the inflow region (see Figures 4 and 5).

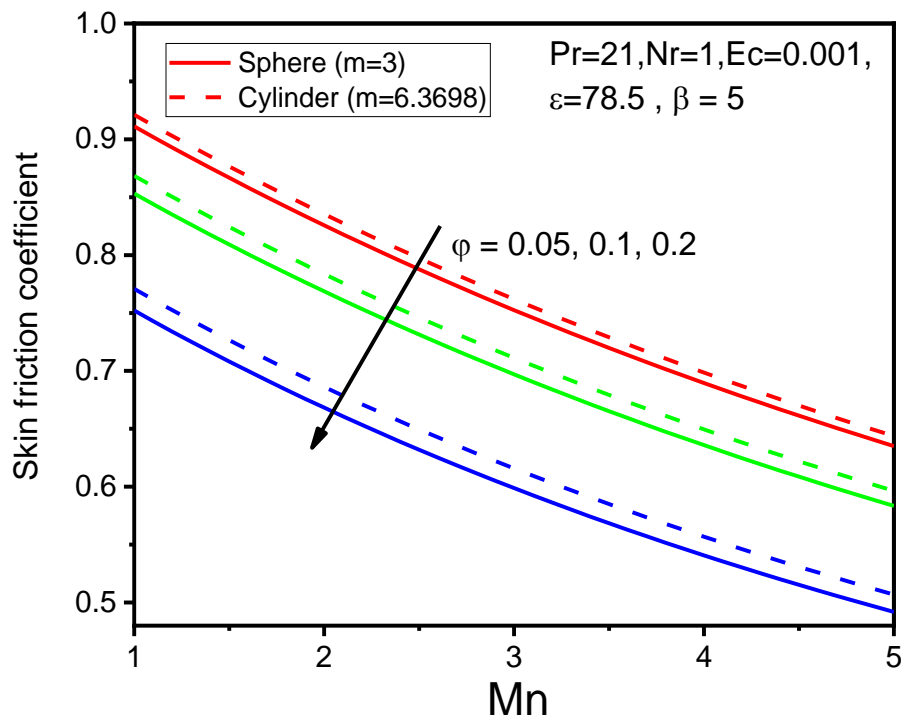


Figure 21. (Case b): Values of the skin friction coefficient for different values of ϕ against Mn .

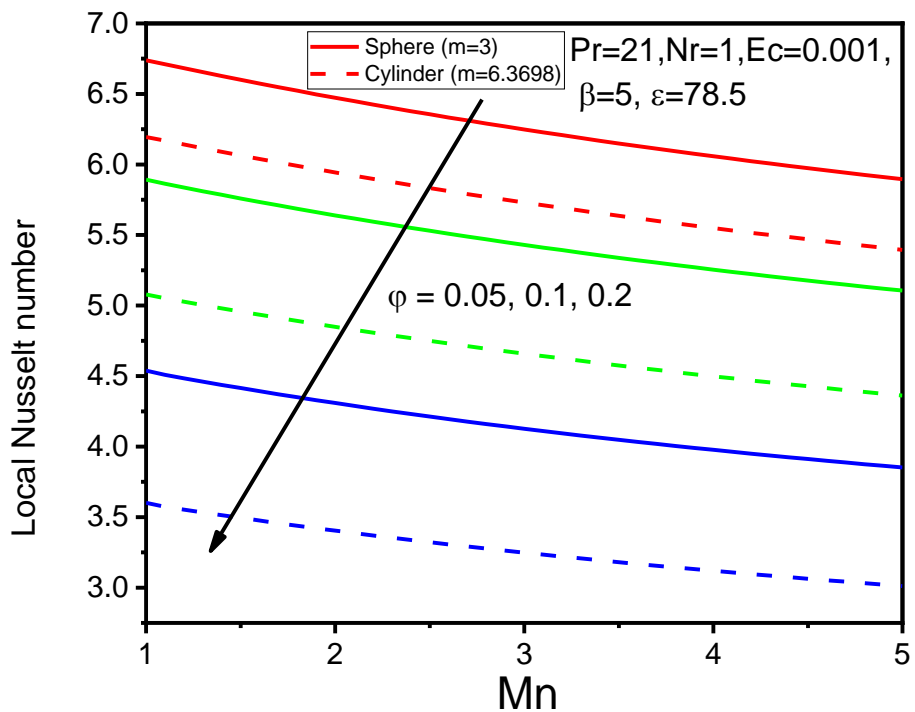


Figure 22. (Case b): Values of the local Nusselt number for different values of ϕ against Mn .

Fluid (blood) velocity decreases for enhancing values of the magnetic field parameter (Figure 8). This is due to the application of the magnetic field which results to the arising of the Lorentz force, acting in the opposite direction to the fluid flow.

Due to the large concentration of magnetic particles, which yields a higher proportion of thermal conductivity, blood temperature is enhanced (see Figure 12) and more significant in case of cylindrical shape.

Additionally, from graphs 17–22, it is observed that the heat transfer rate of blood- Fe_3O_4 is significantly increased by approximately 33.2% compared to that of pure blood, whereas the coefficient of skin friction is reduced by approximately 6.82%. Moreover, the coefficient of skin friction of blood- Fe_3O_4 is increased by approximately 1.09% when particles are in cylindrical shape compared to that of spherical shape, whereas the rate of heat transfer is enhanced 0.08% for spherical shape compared to that of cylindrical shape.

8. Concluding Remarks

In this paper, a BFD model is utilized to study blood flow with magnetic particles under consideration of FHD and MHD principles over a two-dimensional cylinder. The full form of a group theoretical method, namely a two-parameter group theory, is also applied. The effect of thermal radiation is also taken into consideration. With the application of the two-parameter group theory, the number of independent variables is reduced to one variable and, consequently, the set of PDEs is converted into a set of ODEs subject to corresponding boundary conditions. This resultant system of ODEs subject to analogous boundary conditions is numerically solved by applying an efficient numerical technique that consists of a common finite differences method with central differencing, tridiagonal matrix manipulation, and finally an iterative procedure. The significant impact of the variation of the appearing physical parameters is discussed and analogous graphical representations are also demonstrated. Moreover, a comparison of results with others, previously published, is performed to assure the accuracy of the applied numerical algorithm. From the above analysis, we found that:

1. The blood velocity is appreciably reduced, and temperature is significantly improved when magnetic particles are injected into a blood flow stream compared to that of pure blood, where the ferromagnetic interaction parameter plays a significant role.
2. The particle shape plays a vital role in the flow and heat characteristics of blood- Fe_3O_4 , where a better temperature enhancement is observed for cylindrical shapes compared to that of spherical shapes.
3. An increase in the values of the magnetic field parameter and/or the volume of the fraction of the magnetic particles reduced the fluid velocity, whereas for the increment of the ferromagnetic interaction parameter, the fluid velocity was enhanced.
4. The temperature distributions of the fluids increased for all cases of the variation of parameters such as the ferromagnetic interaction parameter, the magnetic field parameter, and the magnetic particle volume fraction.
5. Both velocity and temperature profiles are increased as the values of the radiation parameter are enhanced, whereas the reverse trend is observed as the Eckert number is increased.
6. Both the skin friction coefficient and the rate of heat transfer are escalated with increasing values of the ferromagnetic interaction parameter. The heat transfer rate of blood- Fe_3O_4 is enhanced by approximately 33.2% compared to that of pure blood and the coefficient of skin friction is reduced by approximately 6.82%.
7. Both the coefficient of skin friction and the rate of heat transfer decrease with increasing values of the particle volume fraction. It was found that the skin friction coefficient is increased by approximately 1.09% for cylindrical shapes compared to that spherical shapes, while an 0.08% reduction is noticed for cylindrical shapes in the heat transfer rate compared to spherical shapes.

Author Contributions: Conceptualization, M.F.; Data curation, J.A.; Formal analysis, E.N.P.; Investigation, J.A.; Methodology, G.M. and M.F.; Project administration, E.E.T. and M.F.; Software, J.A., G.M. and E.E.T.; Supervision, E.E.T. and M.F.; Validation, G.M. and E.N.P.; Writing—original draft, J.A. and G.M.; Writing—review & editing, E.N.P. and E.E.T. All authors have read and agreed to the published version of the manuscript.

Funding: This research received no external funding.

Conflicts of Interest: The authors declare no conflict of interest.

List of Symbols

(\bar{u}, \bar{v})	Velocity components [m/s]	\bar{H}	Magnetic field strength [A/m]
(\bar{x}, \bar{r})	Components of the cartesian system [m]	I_1, I_2	Arbitrary function of two-parameter group
R	Radius of the cylinder [m]		
c	Distance between the magnetic dipole and sheet [m]	A, B, C	Arbitrary constants
L	Characteristic length [m]	\bar{T}	Fluid temperature [K]
H_0	Reference magnetic field strength	T_w	Temperature of the cylinder surface [K]
t	Time [s]	T_c	Curie temperature [K]
C_p	Specific heat at constant pressure [$J \text{ Kg}^{-1} \text{ K}^{-1}$]	Mn	Magnetic field parameter
F'	Dimensionless velocity component	K	Pyromagnetic coefficient [K^{-1}]
γ	Strength of the magnetic field at the source position	Ec	Eckert number
Pr	Prandtl number	Nu	Local Nusselt number
α_i, δ_i	Arbitrary constants	C_f	Skin friction coefficient
q_r	Radiative heat flux	B	Magnetic induction
q_w	wall heat transfer parameter	V	Scalar potential of the magnetic dipole
ϕ	Dimensionless magnetic particle volume fraction	ψ	Stream function
η	Dimensionless similarity variable	ρ	Fluid density [Kg/m^3]
θ	Dimensionless temperature	μ	Dynamic viscosity [Kg/ms]
μ_0	Magnetic fluid permeability [NA^{-2}]	v	Kinematical viscosity [m^2/s]
ϵ_1	Convergence criteria	ϵ	Dimensionless Curie temperature
β	Ferromagnetic interaction parameter	κ	Thermal conductivity [$\text{J}/\text{m s K}$]
M	Magnetization	Nr	Thermal radiation parameter
τ_w	Wall shear stress	m	Magnetic particle's shape factor
σ_1	Stefan–Boltzmann constant	σ	Electrical conductivity
χ	Mean absorption coefficient	C_i	Arbitrary coefficient
$(\cdot)_{mf}$	Magnetic fluid	$(\cdot)'$	Base fluid
$(\cdot)_s$	Magnetic particles	v_f	Differentiation with respect to η
(\cdot)	Dimensional quantities		Kinematic viscosity of the fluid

Abbreviations

BFD	Biomagnetic fluid dynamics
FHD	Ferrohydrodynamics
MHD	Magnetohydrodynamic
MRI	Magnetic resonance imaging
PDEs	Partial differential equations
ODEs	Ordinary differential equations

References

1. Stark, D.D.; Weissleder, R.; Elizondo, G.; Hahn, P.F.; Saini, S.; Todd, L.E.; Wittenberg, J.; Ferrucci, J.T. Superparamagnetic iron oxide: Clinical application as a contrast for MR imaging of the liver. *Radiology* **1988**, *168*, 297–301. [[CrossRef](#)]
2. Rugge, E.K.; Rusetski, A.N. Magnetic fluids as drug carriers: Targeted transport of drugs by a magnetic field. *J. Magn. Magn. Mater.* **1993**, *122*, 335–339. [[CrossRef](#)]
3. Fiorentini, G.; Szasz, S. Hyperthermia today: Electric energy, a new opportunity in cancer treatment. *J. Cancer Res. Ther.* **2006**, *2*, 41–46. [[CrossRef](#)]
4. Misra, J.C.; Sinha, A.; Shit, G.C. Flow of a biomagnetic viscoelastic fluid: Application to estimation of blood flow in arteries during electromagnetic hyperthermia, a therapeutic procedure for cancer treatment. *Appl. Math. Mech.-Engl. Ed.* **2010**, *31*, 1405–1420. [[CrossRef](#)]
5. Chien, S.; Usami, S.; Skalsk, R. Blood flow in small tubes. In *American Physiological Society Handbook of Physiology; Section 2, The Cardiovascular System, 4*; Renkins, E.M., Michel, C.C., Eds.; American Physiological Society: Bethesda, MD, USA, 1984; pp. 217–249.
6. Bhatti, M.M.; Abbas, M.A. Simultaneously effects of slip and MHD on peristaltic blood flow of Jeffrey fluid model through a porous medium. *Alex. Eng. J.* **2016**, *55*, 1017–1023. [[CrossRef](#)]
7. Haik, Y.; Chen, J.C.; Pai, V.M. Development of bio-magnetic fluid dynamics. In *Proceedings of the IX International Symposium on Transport Properties in Thermal Fluids Engineering, Singapore*; Winoto, S.H., Chew, Y.T., Wijeyasundera, N.E., Eds.; Pacific Center of Thermal Fluid Engineering: Hawaii, HI, USA, 1996; pp. 121–126.

8. Tzirtzilakis, E.E. A mathematical model for blood flow in magnetic field. *Phys. Fluids* **2005**, *17*, 077103. [[CrossRef](#)]
9. BSharma, K.; Kumawat, C. Impact of temperature dependent viscosity and thermal conductivity on MHD blood flow through a stretching surface with ohmic effect and chemical reaction. *Nonlinear Eng.* **2021**, *10*, 255–271. [[CrossRef](#)]
10. Misra, J.C.; Shit, G.C. Biomagnetic viscoelastic fluid over a stretching sheet. *Appl. Math. Comput.* **2009**, *210*, 350–361. [[CrossRef](#)]
11. Koppu, S.; Pol, B.A.R.; Bhuvanagiri, S.R.V.P. Effects of chemical reaction and thermal radiation on MHD flow over an inclined permeable stretching surface with non-uniform heat source/sink: An application to the dynamics of blood flow. *J. Mech. Med. Biol.* **2014**, *14*, 1450067.
12. Murtaza, M.G.; Tzirtzilakis, E.E.; Ferdows, M. A duality of biomagnetic fluid flow and heat transfer over a quadratic stretched surface. *J. Power Technol.* **2021**, *101*, 154–162.
13. Murtaza, M.G.; Tzirtzilakis, E.E.; Ferdows, M. Effect of electrical conductivity and magnetization on the biomagnetic fluid flow over a stretching sheet. *Z. Angew. Math. Phys.* **2017**, *68*, 93. [[CrossRef](#)]
14. Choi, S.U.S.; Eastman, J.A. Enhancing thermal conductivity of fluids with nanoparticles. In *Developments and Applications of Non-Newtonian Flows*; Siginer, D.A., Wang, H.P., Eds.; ASME: New York, NY, USA, 1995; Volume 66, pp. 99–105.
15. Alsenafi, A.; Ferdows, M. Dual solution for double-diffusive mixed convection opposing flow through a vertical cylinder saturated in a Darcy porous media containing gyrotactic microorganisms. *Sci. Rep.* **2021**, *11*, 19918. [[CrossRef](#)]
16. Nikelham, A.; Enjilela, V.; Vaziri, N.; Moziraji, Z.P. The effects of magnetic-field direction and magnitude on forced convection of aluminum oxide–water nanofluid over a circular cylinder. *Int. J. Therm. Sci.* **2022**, *173*, 107398. [[CrossRef](#)]
17. Aminian, E.; Moghadasi, H.; Saffari, H. Magnetic field effects on forced convection flow of a hybrid nanofluid in a cylinder filled with porous media: A numerical study. *J. Therm. Anal. Calorim.* **2020**, *141*, 2019–2031. [[CrossRef](#)]
18. Tlili, I.; Khan, W.A.; Ramadan, K. MHD flow of nanofluid flow across horizontal circular cylinder: Steady forced convection. *J. Nanofl.* **2019**, *8*, 179–186. [[CrossRef](#)]
19. Elbashbeshy, E.M.A.; Emam, T.G.; El-Azab, M.S.; Abdelgaber, K.M. Effect of magnetic field on flow and heat transfer over a stretching horizontal cylinder in the presence of a heat source/sink with suction/injection. *J. Appl. Mech. Eng.* **2012**, *1*, 1–5. [[CrossRef](#)]
20. Roy, N.; Akter, A. Heat transfer enhancement and boundary layer separations for a hybrid nanofluid flow past an isothermal cylinder. *J. Appl. Comput. Mech.* **2021**, *7*, 2096–2112.
21. Ali, L.; Ali, B.; Ghori, M.B. Melting effect on Cattaneo–Christov and thermal radiation features for aligned MHD nanofluid flow comprising microorganisms to the leading edge: FEM approach. *Comput. Math. Appl.* **2022**, *109*, 260–269. [[CrossRef](#)]
22. Kumar, P.; Poonia, H.; Ali, L.; Areekara, S. The numerical simulation of nanoparticle size and thermal radiation with the magnetic field effect based on tangent hyperbolic nanofluid flow. *Case Stud. Therm. Eng.* **2022**, *37*, 102247. [[CrossRef](#)]
23. Dawar, A.; Saeed, A.; Kumam, P. Magneto-hydrothermal analysis of copper and copper oxide nanoparticles between two parallel plates with Brownian motion and thermophoresis effects. *Int. Commun. Heat Mass Transf.* **2022**, *133*, 105982. [[CrossRef](#)]
24. Bilal, M.; El Ahmed, A.; El-Nabulsi, R.A.; Ahammad, N.A.; Alharbi, K.A.M.; Elkoth, M.A.; Anukool, W.; Zedan, A.S.A. Numerical analysis of an unsteady, Electroviscous, Tenary Hybrid nanofluid flow with chemical reaction and activation energy across. *Micromachines* **2022**, *13*, 874. [[CrossRef](#)] [[PubMed](#)]
25. Souayah, B.; Ramesh, K.; Hdheri, N.; Yasmin, E.; Alam, M.W.; Alfares, K.; Yasmin, A. Heat transfer attributes of Gold–Silver–Blood hybrid nanomaterial flow in an EMHD peristaltic channel with activation energy. *Nanomaterials* **2022**, *12*, 1615. [[CrossRef](#)]
26. Alwawi, F.A.; Swalmeh, M.Z.; Sulaiman, I.M.; Yaseen, N.; Alkasasbeh, H.T.; Al-Soub, T.F. Numerical investigation of heat transfer characteristics for blood/water-based nanofluids in free convection about a circular cylinder. *J. Mech. Eng. Sci.* **2022**, *16*, 8931–8942. [[CrossRef](#)]
27. Alam, J.; Murtaza, M.G.; Tzirtzilakis, E.E.; Ferdows, M. Group Method analysis for Blood-Mn-ZnFe₂O₄ flow and heat transfer under ferrohydrodynamics through a stretched cylinder. *Math. Methods Appl. Sci.* **2022**, *1*–21. [[CrossRef](#)]
28. Shinkai, M.; Ito, A. Functional magnetic particles for medical application. *Adv. Biochem. Engin./Biotechnol.* **2004**, *91*, 191–220.
29. Stueber, D.D.; Vilanova, J.; Aponte, I.; Xiao, Z.; Colvin, V.L. Magnetic nanoparticles in Biology and Medicine: Past, present and future trends. *Pharmaceutics* **2021**, *13*, 943. [[CrossRef](#)] [[PubMed](#)]
30. Ramanujan, V. Magnetic particles for biomedical applications. In *Biomedical Materials*; Narayan, R., Ed.; Springer: Boston, MA, USA, 2009.
31. Baki, A.; Weikhorst, F.; Bleul, R. Advances in magnetic nanoparticles engineering for biomedical applications—A Review. *Bioengineering* **2021**, *8*, 134. [[CrossRef](#)] [[PubMed](#)]
32. Morgan, A.J.A. The reduction by one of the number of independent variables in systems of partial differential equations. *Quart. J. Math. Oxford Ser.* **1952**, *3*, 250–259. [[CrossRef](#)]
33. El-Kabeir, S.M.M.; El-Hakiem, M.A.; Rashad, A.M. Group method analysis for the effect of radiation on MHD coupled heat and mass transfer natural convection flow water vapor over a vertical cone through porous medium. *Int. J. Appl. Math. Mech.* **2007**, *3*, 35–53.
34. Abd-el-Malek, M.B.; Badran, N.B. Group method analysis of unsteady free convective laminar boundary layer flow on a nonisothermal vertical circular cylinder. *Acta Mech.* **1990**, *85*, 193–206. [[CrossRef](#)]
35. Ibrahim, F.S.; Hamad, M.A.A. Group method analysis of mixed convection boundary-layer flow of a micropolar fluid near a stagnation point on a horizontal cylinder. *Acta Mech.* **2006**, *181*, 65–81. [[CrossRef](#)]

36. Rajput, G.R.; Krishnaprasad, J.S.V.R.; Timol, M.G. Group theoretic technique for MHD forced convection laminar boundary flow of nanofluid over a moving surface. *Int. J. Heat Tech.* **2016**, *34*, 1–6. [[CrossRef](#)]
37. Abd-el-Malek, M.B.; Badran, N.A. Group method analysis of steady free-convective laminar boundary-layer flow on a nonisothermal vertical circular cylinder. *J. Comput. Appl. Math.* **1991**, *36*, 227–238. [[CrossRef](#)]
38. Tzirtzilakis, E.E.; Kafoussias, N.G. Three-dimensional magnetic fluid boundary layer flow over a linearly stretching sheet. *J. Heat Transf.* **2010**, *132*, 011702. [[CrossRef](#)]
39. Tzirtzilakis, E.E.; Kafoussias, N.G. Biomagnetic fluid flow over a stretching sheet with non linear temperature dependent magnetization. *Z. Angew. Math. Phys.* **2003**, *54*, 551–565.
40. Tzirtzilakis, E.E.; Tanoudis, G.B. Numerical study of biomagnetic fluid flow over a stretching sheet with heat transfer. *Internat. J. Numer. Methods Heat Fluid Flow* **2003**, *13*, 830–848. [[CrossRef](#)]
41. Raptis, A. Flow of a micropolar fluid past a continuously moving plate by the presence of radiation. *Int. J. Heat Mass Tran.* **1998**, *41*, 2865–2866. [[CrossRef](#)]
42. Raptis, A. Radiation and free convection flow through a porous medium. *Int. Commun. Heat Mass Tran.* **1998**, *25*, 289–295. [[CrossRef](#)]
43. Andersson, H.I.; Valnes, O.A. Flow of a heated ferrofluid over a stretching sheet in the presence of a magnetic dipole. *Acta Mech.* **1998**, *128*, 39–47. [[CrossRef](#)]
44. Nadeem, S.; Ullah, N.; Khan, A.U.; Akbar, T. Effect of homogeneous-heterogeneous reactions on ferrofluid in the presence of magnetic dipole along a stretching cylinder. *Results Phys.* **2017**, *7*, 3574–3582. [[CrossRef](#)]
45. Matsuki, H.; Yamasawa, K.; Murakami, K. Experimental consideration on a new automatic cooling device using temperature sensitive magnetic fluid. *IEEE Trans. Magn.* **1997**, *13*, 1143–1145. [[CrossRef](#)]
46. Makinde, O.D. Stagnation point flow with heat transfer and temporal stability of ferrofluid past a permeable stretching/shrinking. *Defect Diffus. Forum* **2018**, *387*, 510–522. [[CrossRef](#)]
47. Lin, Y.; Zheng, L.; Chen, G. Unsteady flow and heat transfer of pseudo-plastic nano liquid in a finite thin film on a stretching surface with variable thermal conductivity and viscous dissipation. *Powder Technol.* **2015**, *274*, 324–332. [[CrossRef](#)]
48. Kandasamy, R.; Adnan, N.A.-b; Mohammad, R. Nanoparticles shape effects on squeezed MHD flow of water based on Cu, Al₂O₃ and SWCNTs over a porous sensor surface. *Alex. Eng. J.* **2018**, *57*, 1433–1445. [[CrossRef](#)]
49. Alam, J.; Murtaza, G.; Tzirtzilakis, E.E.; Ferdows, M. Biomagnetic fluid flow and heat transfer study of blood with gold nanoparticles over a stretching sheet in the presence of magnetic dipole. *Fluids* **2021**, *6*, 113. [[CrossRef](#)]
50. Aziz, A.; Jamshed, W.; Ali, Y.; Shams, M. Heat transfer and entropy analysis of Maxwell hybrid nanofluid including effects of an inclined magnetic field, Joule heating and thermal radiation. *Discrete Contin. Dyn. Syst. Ser. S* **2020**, *13*, 2667–2690. [[CrossRef](#)]
51. Reddy, S.R.R.; Reddy, P.B.A. Bio-mathematical analysis for the stagnation point flow over a non-linear stretching surface with the second order velocity slip and titanium alloy nanoparticle. *Front. Heat Mass Tran.* **2018**, *10*, 13.
52. Hassanien, I.A.; Salama, A.A.; Hosham, H.I. Group theoretic method analysis for unsteady boundary layer flow near a stagnation point. *Taiwanese J. Math.* **2005**, *9*, 639–660. [[CrossRef](#)]
53. Abd-el-Malek, M.B.; Boutros, Y.Z.; Badran, N.A. Group method analysis of unsteady free-convective laminar boundary-layer flow on a nonisothermal vertical flat plate. *J. Engrg. Math.* **1990**, *24*, 343–368. [[CrossRef](#)]
54. Moran, M.J.; Gaggioli, R.A. A new systematic formalism for similarity analysis with application to boundary layer flows. *U.S. Army Math. Res. Center Tech. Summ.* **1968**, *75*, AD0681404.
55. Moran, M.J.; Gaggioli, R.A. A new systematic formalism for similarity analysis. *J. Engrg. Math.* **1969**, *3*, 151–162. [[CrossRef](#)]
56. Kafoussias, N.G.; Williams, E.W. An improved approximation technique to obtain numerical solution of a class of two-point boundary value similarity problems in fluid mechanics. *Int. J. Numer. Meth. Fluids* **1993**, *17*, 145–162. [[CrossRef](#)]
57. Alam, M.J.; Murtaza, M.G.; Tzirtzilakis, E.E.; Ferdows, M. Effect of thermal radiation on biomagnetic fluid flow and heat transfer over an unsteady stretching sheet. *Comput. Assist. Meth. Eng. Sci. (CAMES)* **2021**, *28*, 81–104.
58. Fenuga, O.J.; Hasan, A.R.; Olanrewaju, P.O. Effects of radiation and Eckert number on MHD flow with heat transfer rate near a stagnation point over a non-linear vertical stretching sheet. *Int. J. Appl. Mech. Eng.* **2020**, *25*, 27–36. [[CrossRef](#)]